Cell Reports

Article

Satb1 directs the differentiation of T_H17 cells through suppression of IL-2 expression

Graphical abstract

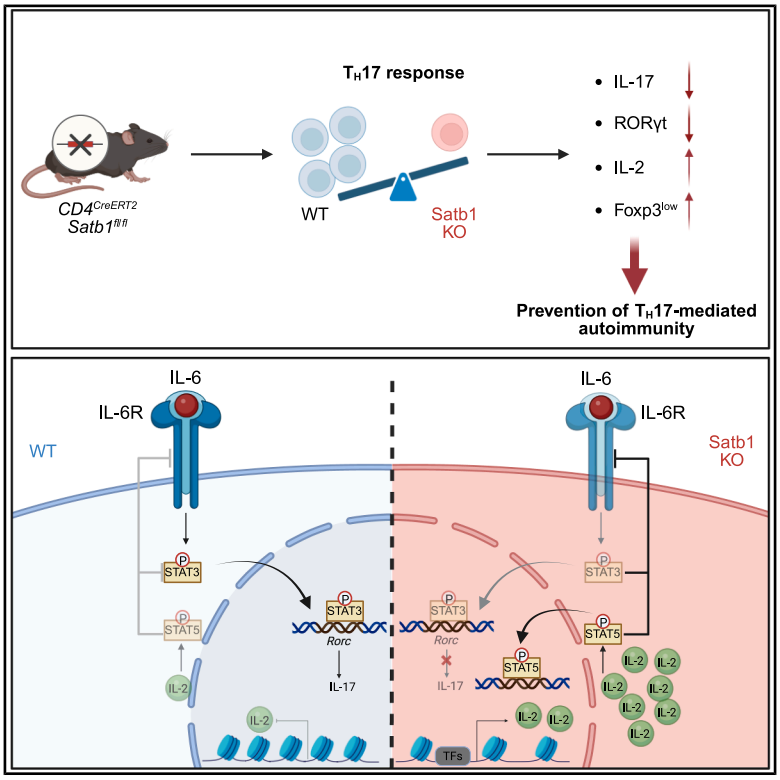

Highlights

- Satb1 deletion inhibits T_H17 cell differentiation *in vitro* and *in vivo*
- Loss of Satb1 prevents T_H17 cell-mediated autoimmunity
- Satb1 is a key regulator of IL-2 expression in naive $CD4^+$ T cells
- Satb1 deficiency via increased IL-2/STAT5 signaling prevents T_H17 cell development

Authors

Maren Köhne, Mehrnoush Hadaddzadeh Shakiba, Lisa Schmidleithner, ..., Simon C. Barry, Joachim L. Schultze, Marc D. Beyer

Correspondence

marenkoehne@outlook.de (M.K.), marc.beyer@dzne.de (M.D.B.)

In brief

Satb1 has a key role in T cell development and differentiation. In this study, Köhne et al. showed that deletion of Satb1 in naive $CD4^+$ T cells inhibits T_H17 cell development via alterations in IL-2/STAT5 signaling preventing T_H17 cell-driven autoimmunity *in vivo* in the EAE and experimental colitis model.

Köhne et al., 2025, Cell Reports *44*, 115866
July 22, 2025
https://doi.org/10.1016/j.celrep.2025.115866

CellPress

Cell Reports

CellPress
OPEN ACCESS

Article

Satb1 directs the differentiation of T_H17 cells through suppression of IL-2 expression

Maren Köhne,[1,18,*] Mehrnoush Hadaddzadeh Shakiba,[1,18] Lisa Schmidleithner,[1] Jonas Schulte-Schrepping,[2,3] Rebekka Scholz,[1] Tarek Elmzzahi,[1,4] Daniel Sommer,[2] Yuanfang Li,[1] Caterina Carraro,[2,3] Elena De Domenico,[2,5] Jannis Wißfeld,[2,6] Kristian Händler,[2,5,7] Doaa Hamada,[1,8] Aleksej Frolov,[1,4] Xiaoxiao Cheng,[1] Ann-Kathrin Baumgart,[9] Lisa Holsten,[2,3] Collins Osei-Sarpong,[1] Svenja Bourry,[1] Yasser Thabet,[2] Hannes Renken,[10] Stefan Paulusch,[3,5] Timothy Sadlon,[11] Thorsten Buch,[12] F. Thomas Wunderlich,[13] Claudia Wickenhauser,[14] Judith Alferink,[10,15] Tanja Kuhlmann,[16] Matthias Geyer,[17] Lorenzo Bonaguro,[2,3] Simon C. Barry,[11] Joachim L. Schultze,[2,3,5] and Marc D. Beyer[1,3,5,19,*]

[1]Immunogenomics & Neurodegeneration, German Center for Neurodegenerative Diseases (DZNE), 53127 Bonn, Germany
[2]Genomics and Immunoregulation, Life & Medical Sciences (LIMES) Institute, University of Bonn, 53115 Bonn, Germany
[3]Systems Medicine, German Center for Neurodegenerative Diseases (DZNE), 53127 Bonn, Germany
[4]Department of Microbiology and Immunology, The Peter Doherty Institute for Infection and Immunity, University of Melbourne, Melbourne, VIC, Australia
[5]Platform for Single Cell Genomics and Epigenomics at the German Center for Neurodegenerative Diseases (DZNE) and the University of Bonn and West German Genome Center, 53127 Bonn, Germany
[6]Division of mRNA Cancer Immunotherapies, Helmholtz Institute for Translational Oncology (HI-TRON) Mainz, 55131 Mainz, Germany
[7]Institute of Human Genetics, Universitätsklinikum Schleswig-Holstein, University of Lübeck and University of Kiel, 23562 Lübeck, Germany
[8]Medical Microbiology and Immunology Department, Faculty of Medicine, Mansoura University, 35511 Mansoura, Egypt
[9]Institute of Molecular Medicine and Experimental Immunology, University Hospital Bonn, 53127 Bonn, Germany
[10]Department of Psychiatry, University of Münster, 48149 Münster, Germany
[11]Molecular Immunology, Robinson Research Institute, University of Adelaide, North Adelaide, SA 5006, Australia
[12]Institute of Laboratory Animal Science, University of Zurich, Schlieren, 8952 Zurich, Switzerland
[13]Max Planck Institute for Metabolism Research, Center for Endocrinology, Diabetes and Preventive Medicine (CEDP), 50931 Cologne, Germany
[14]Institute for Pathology, Martin-Luther University Halle - Wittenberg, 06112 Halle (Saale), Germany
[15]Cells in Motion Interfaculty Cluster, University of Münster, Münster, Germany
[16]Institute for Neuropathology, University Hospital Münster, 48149 Münster, Germany
[17]Institute of Structural Biology, University of Bonn, 53127 Bonn, Germany
[18]These authors contributed equally
[19]Lead contact
*Correspondence: marenkoehne@outlook.de (M.K.), marc.beyer@dzne.de (M.D.B.)
https://doi.org/10.1016/j.celrep.2025.115866

SUMMARY

T helper (T_H)17 cells are crucial for host defense in barrier organs, and their altered functionality can disrupt tissue homeostasis, increasing the risk of autoimmune diseases. Thus, it is essential to understand the mechanisms controlling T_H17 differentiation to develop strategies influencing their role in diseases. Here, we identified Special AT-rich sequence-binding protein 1 (Satb1) as a pioneering factor for T_H17 development. Satb1 is highly expressed in T_H17 cells, and loss of Satb1 prevents the differentiation of T_H17 cells. Consequently, expression of Satb1 in $CD4^+$ T cells is required for the formation of T_H17-driven autoimmune diseases. Mechanistically, Satb1 mediates T_H17 development through regulating accessibility of the *Il2* gene locus and thereby preventing interleukin (IL)-2 signaling early during T_H17 differentiation. Hence, suppression of IL-2 expression by Satb1 during T_H17 formation is pivotal, suggesting that Satb1 could serve as a novel therapeutic target for treating autoimmune diseases driven by T_H17 cells.

INTRODUCTION

T helper (T_H)17 cells are essential for tissue homeostasis and inflammation by preventing invasion and clearing extracellular pathogens.[1] Beyond their protective role, they contribute to autoimmune diseases like multiple sclerosis and inflammatory bowel disease,[2] reflecting diverse effector functions[3] and distinct T_H17 functional states.[4] T_H17 cells differentiate in response to interleukin (IL)-6 and transforming growth factor (TGF)-β1, with IL-6 signaling activating signal transducer and activator of transcription 3 (Stat3), which induces RAR-related orphan receptor gamma (RORγt) and initiates the T_H17 gene program. Secretion of IL-17 and IL-22 enhances immune responses in epithelial and stromal cells, leading to neutrophil recruitment

and antimicrobial peptide production.[1] Additionally, IL-23 signaling and TGF-β3 expression are crucial for the emergence of pathogenic features and the progression of T_H17-driven autoimmune diseases.[5,6] More recently, a role for Special AT-rich sequence-binding protein 1 (Satb1) in pathogenic T_H17 effector function has been ascribed.[7,8] Satb1, a chromatin organizer and transcription factor, is essential for lymphocyte development and function.[9] Satb1 modulates gene expression through formation of high-order chromatin loop structures enabling long-range interactions[10–14] and by recruiting chromatin-modifying factors to target loci.[15] Thus, Satb1 shapes the nuclear architecture and epigenetic landscape, acting both as an activator and repressor. Satb1 plays multiple roles in T cell development, promoting lymphoid lineage commitment from hematopoietic stem cells (HSCs) and guiding thymocyte maturation, including T cell receptor (TCR)α rearrangement, thymic development, and $CD4^+/CD8^+$ lineage decisions.[9,16–25]

In peripheral $CD4^+$ T cells, Satb1 promotes CD25 and IL-2 expression in conventional T cells (T_{conv}) cells.[26] During T_H cell differentiation, Satb1 supports T_H2 lineage commitment by restructuring the T_H2 cytokine locus and inducing Gata3 expression.[27–29] Additionally, Satb1 deficiency in tumor settings correlates with increased follicular T_H (T_{FH}) cell formation.[30] Furthermore, downregulation of Satb1 fosters the development of peripheral regulatory T (pT_{reg}) cells and is required for the suppressive function of regulatory T (T_{reg}) cells and for the maintenance of a T_{reg} phenotype.[20,31,32] *In silico* analyses identified Satb1 as a key regulator for T_H17 cells,[33,34] supported by studies in experimental autoimmune encephalomyelitis (EAE) showing its regulation of granulocyte-macrophage colony-stimulating factor (GM-CSF) and programmed cell death protein 1 (PD-1) expression in T_H17 cells.[7,8] However, the precise cellular and molecular mechanisms by which Satb1 contributes to autoimmunity remain unclear. Understanding the role of Satb1 in peripheral T cells has been limited by genetic models like CD4-Cre and Thpok-Cre, which delete Satb1 before thymic egress, confounding peripheral effects with thymic development. To overcome this, we used a tamoxifen-inducible model to delete Satb1 specifically in peripheral T cells, combined with functional, epigenomic, and transcriptional analyses. We identify a role for Satb1 early in T_H17 differentiation, where it suppresses IL-2 to promote the T_H17 gene program. Peripheral deletion of Satb1 disrupts this program and confers complete protection from autoimmune diseases such as EAE and experimental colitis.

RESULTS

Satb1 is required for T_H17 cell differentiation and function

As Satb1 was previously linked specifically to T_H17 cells,[33,34] we first analyzed its expression across $CD4^+$ T cell subsets. Under homeostatic conditions, Satb1 was expressed in $CD4^+CD44^-CD62L^+CD25^-$ naive T cells and downregulated in $CD4^+CD44^+CD62L^-CD25^-$ effector/memory T cells at the mRNA (Figure S1A) and protein level (Figures S1B and S1C). Furthermore, *in vitro* differentiation showed Satb1 was most strongly upregulated in T_H17 cells compared to naive and other T_H cell subsets (Figures S1D–S1F), indicating a key role in T_H17 differentiation. To identify regulators of Satb1, we analyzed datasets from Stat3- and RORγt-deficient T_H17 cells and found both factors bind to the genomic *Satb1* locus (Figure S1G). However, only Stat3 deficiency significantly reduced Satb1 mRNA, while RORγt loss had no effect (Figure S1H).

To explore a causal link between Satb1 induction and T cell differentiation, we used a conditional Satb1-deficient mouse line.[35] This model expresses enhanced green fluorescent protein (eGFP) under the control of the Satb1 promoter post recombination, mirroring endogenous Satb1 levels (Figure S1I). Given the role of Satb1 in thymic T cell development,[19–21] we crossed these mice with CD4-CreERT2 mice,[36] enabling tamoxifen-inducible Satb1 deletion in mature peripheral $CD4^+$ T cells. Tamoxifen treatment in adult mice led to Satb1 loss in naive $CD4^+$ T cells, which instead expressed high eGFP, while effector/memory $CD4^+$ T cells showed low eGFP expression (Figures S1J–S1N).

To investigate the impact of Satb1 on T_H cell generation, we performed *in vitro* differentiation of Satb1-sufficient and -deficient naive $CD4^+$ T cells into T_H1, T_H2, T_H17, and induced regulatory T cells (iT_{reg}) cells. Satb1 deficiency led to reduced T_H2 differentiation and increased iT_{reg} and T_H1 differentiation (Figures S1O–S1S), with the most striking effect seen in T_H17 cells. Knockout (KO) $CD4^+$ T cells failed to express IL-17 at both mRNA and protein level under T_H17 conditions (Figures 1A and 1B), and RORγt expression was completely lost (Figure 1C) indicating Satb1 is critical for T_H17 differentiation. To ensure this was not due to skewing toward other lineages, we assessed T_H1, T_H2, and iT_{reg} cell markers and found no aberrant induction under T_H17 conditions (Figure S2A).

T_H cell-fate decisions rely on tightly regulated gene networks. Recent studies have identified both positive and negative regulators of T_H17 differentiation through gene-expression analyses and murine models.[33,34] Given its function as a transcription factor and chromatin organizer, Satb1 likely modulates gene modules involved in T_H17 differentiation. To address this question, we analyzed expression of T_H17 core genes in Satb1-sufficient and -deficient naive $CD4^+$ T cells under T_H17 differentiation conditions. Notably, Satb1-deficient cells showed reduced expression of key positive regulators of T_H17 differentiation, particularly after 12 h of differentiation (Figure 1D). In contrast, negative regulators were unaffected early and only altered at later stages, after differentiation had already been prevented. These findings suggest that Satb1 is essential for T_H17 lineage commitment by initiating the positive gene module required for T_H17 differentiation.

Satb1 has been proposed to influence not only transcription but also metabolic reprogramming.[37] To test whether Satb1 affects T_H17 differentiation also through metabolic regulation, we assessed cellular metabolism. Although Satb1-deficient cells were less metabolically active 3 days after T_H17 induction (baseline oxygen consumption rate [OCR] and extracellular acidification rate [ECAR]; Figures 1E and S2B), both Satb1-sufficient and -deficient cells showed similar respiratory capacity and overall metabolic potential (Figures 1E and 1F). These findings suggest that Satb1 regulates T_H17 differentiation primarily by establishing the required transcriptional networks without

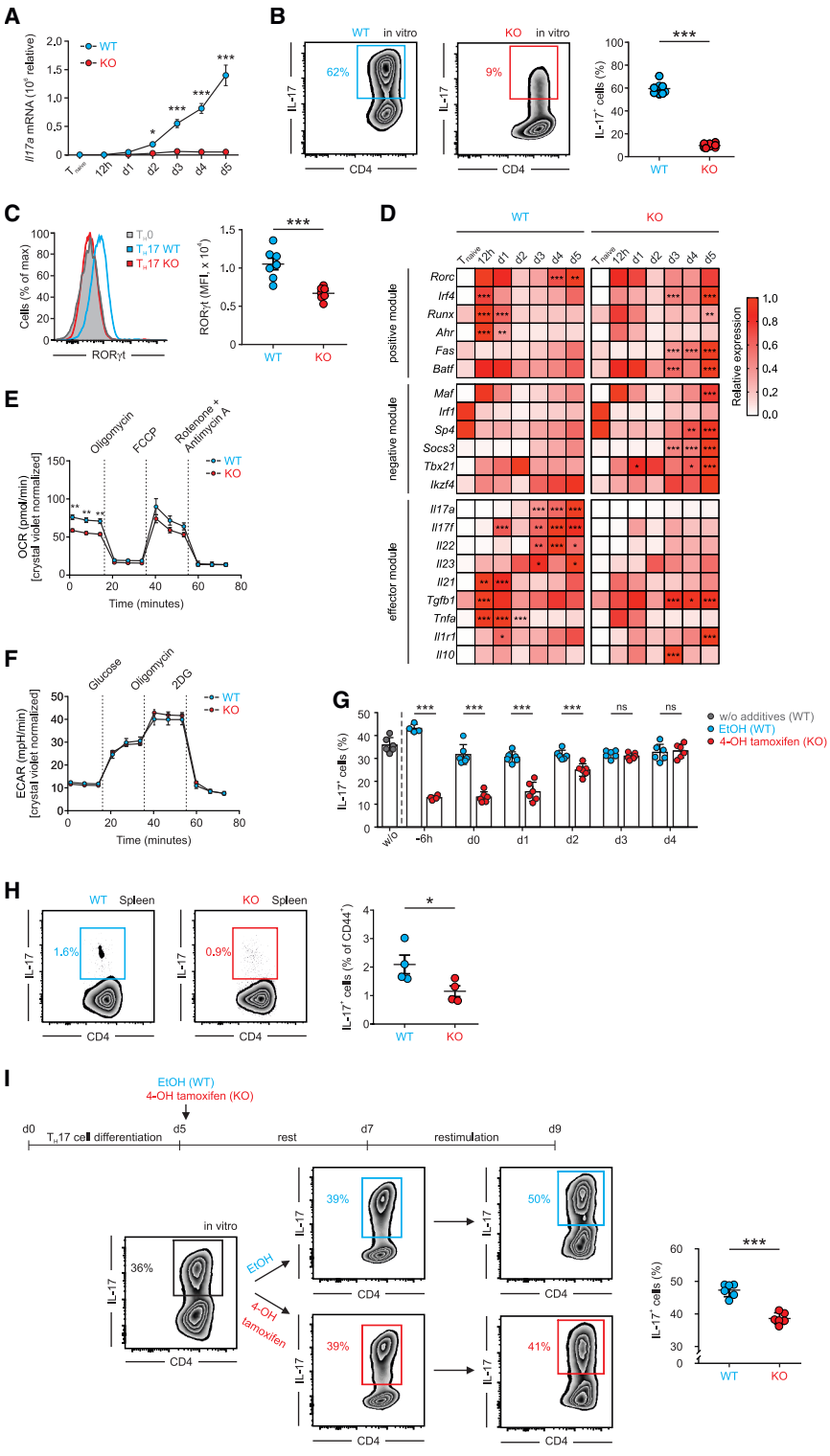

Figure 1. Satb1 regulates the early phase of T_H17 cell differentiation

(A–F) Satb1-sufficient (WT) and -deficient (KO) naive $CD4^+CD44^-CD62L^+CD25^-$ T cells from $Satb1^{fl/fl}$ × CD4-CreERT2 mice were isolated and differentiated *in vitro* into T_H17 cells. (A) *Il17a* mRNA expression over time by RT-qPCR, normalized to β-actin, and shown relative to WT cells (n = 3–5/group). (B) Analysis of IL-17 (n = 8/group) and (C) RORγt protein expression (n = 7/group) by flow cytometry on day 5. (D) Core T_H17 gene expression over time by RT-qPCR, normalized to β-actin and shown relative to the peak time point (n = 3–5/group). (E and F) Metabolic analysis 3 days after T_H17 induction. (E) Oxygen consumption rate (OCR) upon treatment with oligomycin, Carbonyl cyanide-p-trifluoromethoxyphenylhydrazone (FCCP), and rotenone/antimycin A (WT n = 13, KO n = 11, repeated measurement). (F) Extracellular acidification rate (ECAR) upon challenge with glucose, oligomycin, and 2DG (WT n = 13, KO n = 10, repeated measurement).

(G) IL-17 expression after timed deletion of Satb1 during T_H17 differentiation using 4-OH tamoxifen (−6 h to day 4), analyzed by flow cytometry on day 5 (n = 4–6/group).

(H) IL-17 expression in splenic effector/memory $CD4^+$ T cells from aged $Satb1^{fl/fl}$ × $CD4\text{-}Cre^{wt/wt}$ (WT) or $Satb1^{fl/fl}$ × $CD4\text{-}Cre^{wt/+}$ (KO) mice (n = 4/group).

(I) IL-17 expression following Satb1 deletion at day 5 of T_H17 culture, after 2 days resting and 2 days of CD3/CD28 restimulation with T_H17 cytokines, analyzed on days 5, 7, and 9 (n = 6/group).

Data are shown as (A–C and E–I) mean ± SEM and (D) as mean. Significant differences in gene expression between WT and KO cells are shown and illustrated on the higher expressing cells. (A, D, and G) Two-way ANOVA with Sidak's test; (B, C, H, and I) unpaired Student's t test; (E and F) two-way repeated-measures ANOVA with Sidak's multiple-comparison test (ns, not significant, $p \geq 0.05$; $^*p < 0.05$; $^{**}p < 0.01$; $^{***}p < 0.001$). Data are pooled from two independent experiments (C and G), three independent experiments (B), or are representative of two independent experiments (E, F, and H). d, day; EtOH, ethanol; h, hours; MFI, mean fluorescence intensity. See also Figures S1 and S2.

impacting metabolic processes. As Satb1 has been linked to pathogenic effector function of T_H17 cells[7,8]—particularly the co-expression of IL-17 and GM-CSF—we examined GM-CSF expression. Conditional Satb1 deletion prior to initiation of differentiation of naive $CD4^+$ T cells into T_H17 cells abolished GM-CSF expression (Figure S2C). To pinpoint the critical window of Satb1 function, we deleted Satb1 at various time points during T_H17 differentiation (Figure S2D). IL-17 expression was significantly reduced when Satb1 was deleted before day 2, but not at later stages (Figures 1G and S2E). In summary, as deletion of Satb1 before or at early time points of T_H17 cell differentiation had the strongest impact on IL-17 expression, we postulate that Satb1 is important especially during the initial steps of T_H17 cell differentiation.

To further validate our findings, we examined the effects of Satb1 loss *in vivo* by crossing CD4-Cre mice with conditionally Satb1-deficient animals. Aged Satb1$^{fl/fl}$ × CD4-Cre$^{+/wt}$ mice showed increased splenic CD4$^+$ T cell differentiation into effector/memory cells (Figure S2F), consistent with prior results from Satb1$^{fl/fl}$ animals crossed to Vav-Cre mice.[21] However, unlike previous reports,[20,21] we did not observe overt autoimmunity. Spontaneous T_H17 differentiation within the effector/memory pool was reduced in Satb1-deficient mice, aligning with our *in vitro* data (Figure 1H), underscoring the importance of Satb1 for T_H17 differentiation. To explore its role post differentiation, we deleted Satb1 in polarized T_H17 cells and restimulated them via TCR under T_H17 conditions. IL-17 expression increased in Satb1-sufficient but not in Satb1-deficient cells (Figure 1I), indicating Satb1 is also required for mature T_H17 cell function. Collectively, our data established a causal role for Satb1 in both T_H17 differentiation and function.

Loss of Satb1 prevents intestinal inflammation through loss of pathogenic T_H17 cells

Inflammatory bowel diseases (IBDs) can arise from T_H17-mediated pathogenicity.[38–40] Since Satb1 is required for T_H17 differentiation *in vitro* and *in vivo*, we investigated whether Satb1 expression in CD4$^+$ T cells contributes to IBD. We used an experimental colitis model by adoptively transferring Satb1-sufficient or -deficient naive CD4$^+$ T cells into recombination activating gene 2 knockout mice (Rag2$^{-/-}$) (Figure S3A). This approach allows assessment of the intrinsic effect of Satb1 on naive CD4$^+$ T cell differentiation and disease development. Transfer of wild-type (WT) naive CD4$^+$ T cells induced severe colitis, shown by weight loss and colonic infiltration (Figures 2A–2C).[41] In contrast, transfer of Satb1-deficient naive CD4$^+$ T cells failed to induce pathology (Figures 2A–2C) and showed reduced inflammation-driven proliferation in mesenteric lymph nodes (mesLNs) and spleen (Figures 2D, 2E, and S3B). Additionally, Satb1-deficient CD4$^+$ T cells were less activated as indicated by lower CD25 and Ki-67 expression (Figures S3C and S3D). To exclude the possibility that reduced inflammation resulted from increased T_{reg} differentiation since low Satb1 levels are linked to enhanced T_{reg} function,[20,31] we assessed Foxp3 expression. Although the percentage of Foxp3$^+$ CD4$^+$ T cells slightly increased after transfer of Satb1-deficient naive T cells, their total number was significantly lower (Figures 2F, S3E, and S3F), indicating that protection from colitis was not due to enhanced T_{reg} formation. Serum cytokine analysis revealed lower levels of IL-17A, IL-17F, IL-22, interferon (IFN)-γ, tumor necrosis factor (TNF)-α, and IL-6 in Rag2$^{-/-}$ mice receiving Satb1-deficient T cells, while IL-10 levels remained unchanged (Figure 2G). These results show that Satb1 in CD4$^+$ T cells is essential for driving systemic inflammation in lymphopenic hosts, independent of T_{reg} development. To assess how loss of Satb1 affects CD4$^+$ T cell differentiation, we analyzed IL-17 expression and observed reduced T_H17 differentiation in Satb1-deficient cells (Figures 2H and S3G). We then evaluated T_H17 subsets based on IFN-γ co-expression and found lower frequencies and total numbers of both non-pathogenic IL-17$^+$IFN-γ$^-$ and pathogenic IL-17$^+$IFN-γ$^+$ T_H17 cells in the mesLN and spleen of Rag2$^{-/-}$ mice receiving Satb1-deficient naive T cells (Figures 2I and S3H). In contrast, IL-17$^-$IFN-γ$^+$ T_H1 percentages were similar between groups, although absolute numbers were reduced in mice receiving Satb1-deficient cells (Figures 2I and S3H). Analysis of intramural T cells in the colon showed increased frequencies but reduced total numbers of both pathogenic and non-pathogenic T_H17 cells, consistent with the observed pathology (Figures S3I and S3J). Detailed assessment of CD4$^+$ T cell polyfunctionality revealed a significant reduction in cytokine co-expressing cells in mesLN and spleen, but not in the colon, upon Satb1 deletion (Figures 2J, S3K, and S3L). This indicates that Satb1 suppresses colitis by limiting both T_H17 development and CD4$^+$ T cell polyfunctionality in lymphoid tissues, leading to reduced intestinal infiltration and inflammation. Since T_H17 cells recruit neutrophils, we examined neutrophil infiltration and observed reduced myeloid cell and neutrophil numbers in mesLN, spleen, and colon of mice receiving Satb1-deficient T cells (Figures 2K, S3M, and S3N). These results demonstrate that Satb1 is essential for T_H17-mediated colitis by regulating naive CD4$^+$ T cell differentiation.

Satb1 is crucial for T_H17 cell pathogenicity in EAE

Previous studies showed that Satb1 is essential for T_H17 effector function during EAE.[7,8] We investigated whether Satb1 also influences T_H17 development the induction phase of EAE. Using the CD4-CreERT2 model, Satb1 was deleted directly before EAE induction (Figure S4A). Strikingly, mice with Satb1-deficient CD4$^+$ T cells were resistant to EAE, showing no paralysis, weight loss (Figure S4B), or demyelination after myelin oligodendrocyte glycoprotein $(MOG)_{35-55}$/CFA immunization (Figures 3A and 3B). Correspondingly, we observed reduced myeloid and CD4$^+$ T cell infiltration in the brain and spinal cord (Figures 3C and 3D) and decreased cell activation (Figure S4C). Thus, our data support that Satb1 is required for the development of EAE. To determine whether reduced pathology results from impaired T_H17 differentiation in Satb1-deficient CD4$^+$ T cells, we assessed IL-17 and RORγt expression. Fewer T_H17 cells were found in the central nervous system (CNS) and cervical lymph nodes (cLNs) upon Satb1 deletion (Figures 3E, 3F, S4D, and S4E). As pathogenic T_H17 cells are important for disease development,[5,6] we co-stained for IL-17 and IFN-γ and observed reduced frequencies and total numbers of both IL-17$^+$IFN-γ$^-$ and IL-17$^+$IFN-γ$^+$ cells in the CNS and spinal cord (Figures 3G and S4F) and fewer IL-17$^+$IFN-γ$^-$ cells in the cLN (Figure S4G). Since IL-17$^+$IFN-γ$^+$ cells are known to be highly MOG specific,[42] and we saw less pathogenic T_H17 differentiation upon Satb1 deletion, we used $MOG_{38–49}$/I-A^b tetramer staining and found a near-complete loss of MOG-specific CD4$^+$ T cells in Satb1-deficient mice (Figure 3H).

To exclude the possibility that reduced cell expansion and infiltration were due to increased pT_{reg} differentiation, we analyzed Foxp3 and CD25 co-expression in CD4$^+$ T cells. Satb1 deletion led to fewer CD25$^+$Foxp3$^+$ T_{reg} cells in the brain, while frequency of CD25$^-$Foxp3$^+$ cells increased (Figure 3I). As CD25$^-$Foxp3$^+$ cells in Satb1-deficient mice lack typical T_{reg} characteristics[20] and true T_{reg} cells were reduced, resistance to CNS pathology is unlikely to be driven by T_{reg} expansion. Additionally, IL-10$^+$ CD4$^+$ T cell frequencies in the CNS and cLNs were unchanged, while total IL-10$^+$ CD4$^+$ T cell numbers were lower in the CNS after Satb1 deletion (Figures 3J, S4H, and S4I), suggesting IL-10 is not responsible for disease protection.

To assess the heterogeneity of EAE-associated T cells based on Satb1 expression, we performed targeted single-cell RNA

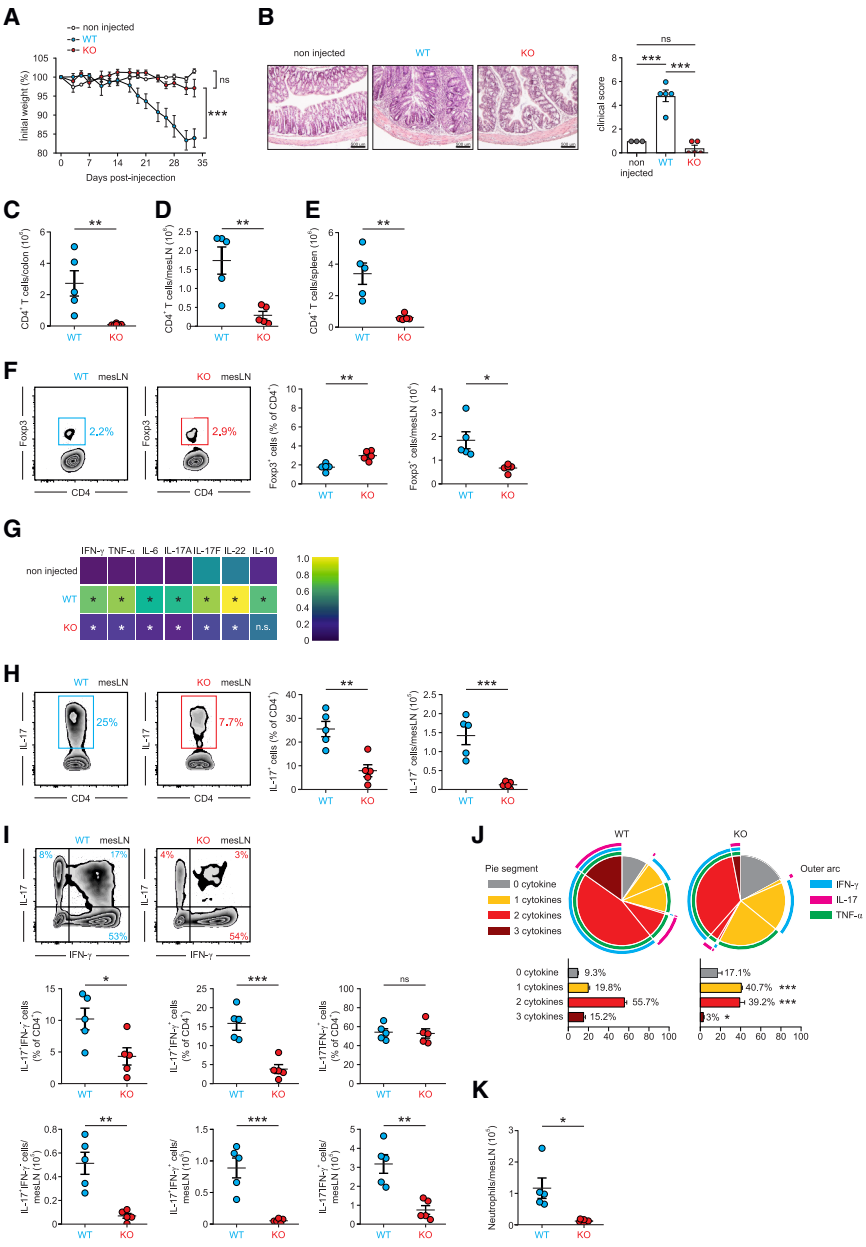

Figure 2. Loss of Satb1 diminishes T_H17 differentiation *in vivo* and prevents the development of $CD4^+$ T cell-mediated adoptive colitis

Analysis of colitis induced by adoptive transfer of Satb1-sufficient (WT) or -deficient (KO) naive $CD4^+$ $CD44^-CD62L^+CD25^-$ T cells from $Satb1^{fl/fl}$ × CD4-CreERT2 mice into $Rag2^{-/-}$ recipients. Data collected ~5 weeks post transfer.

(A) Body weight of $Rag2^{-/-}$ mice over time, normalized to baseline (non-injected $n = 4$, WT $n = 5$, KO $n = 5$).

(B) H&E staining of colon (left) and histology scoring (right) (non-injected $n = 3$, WT $n = 5$, KO $n = 5$). Scale bar, 500 μm.

(C–E) $CD4^+$ T cell counts in colon (n = 5–6/group) (C), mesLN ($n = 5$/group) (D), and spleen ($n = 5$/group) (E) quantified by flow cytometry.

(F) Frequencies and total numbers of $CD4^+Foxp3^+$ T cells in the mesLN ($n = 5$/group).

(G) Serum cytokine levels shown as Z score ($n = 5$/group).

(H) Frequencies and total numbers of $CD4^+IL\text{-}17^+$ T cells in the mesLN ($n = 5$/group).

(I) Frequencies and total numbers of non-pathogenic $CD4^+IL\text{-}17^+IFN\text{-}\gamma^-$ T_H17 cells, pathogenic $CD4^+IL\text{-}17^+IFN\text{-}\gamma^+$ T_H17 cells and $CD4^+IL\text{-}17^-IFN\text{-}\gamma^+$ T_H1 cells in the mesLN ($n = 5$/group).

(J) Cytokine expression (IFN-γ, IL-17, TNF-α) in mesLN $CD4^+$ T cells ($n = 5$/group).

(K) $Ly6G^+$ neutrophil counts in mesLN quantified by flow cytometry ($n = 5$/group).

Data are shown as mean ± SEM. (A) Two-way repeated-measures ANOVA with Tukey's multiple-comparison test; (B) one-way ANOVA with Tukey's multiple-comparison test; (C–F, H, I, and K) unpaired Student's t test; (G) one-way ANOVA with Tukey's multiple-comparison test (comparisons for non-injected vs. WT and WT vs. KO are depicted). (J) two-way ANOVA with Sidak's multiple-comparison test (ns, not significant, $p \geq 0.05$; *$p < 0.05$; **$p < 0.01$; ***$p < 0.001$). (A and C–J) Data are representative of at least three independent experiments. mesLN, mesenteric lymph nodes. See also Figure S3.

sequencing (scRNA-seq) of CNS-derived T cells at peak of disease. We identified nine $CD4^+$ T cell subsets: three T_H1 subsets (TH1a, TH1b, TH1c), three T_H17 subsets (stem-like, TH17a, TH17b), central-memory $CD4^+$ T cells (Tcm), T_{reg} cells, and a proliferating $CD4^+$ T cell population (Figure 3K). Subtype distribution was largely unchanged in Satb1-deficient mice (Figure S4J), and marker gene analysis confirmed prototypical marker expression across subsets (Figure S4K). To determine how Satb1 loss affects transcriptional profiles, we compared gene expression between Satb1-sufficient and -deficient $CD4^+$ T cell clusters and found only a few differentially expressed (DE) genes (Figures 3L and S4L). Notably, genes linked to T cell activation and function such as *Tnf*, *Ifng*, *Tnfrsf4*, and *Tnfrsf9* were downregulated in Satb1-deficient cells (Figure 3M), consistent with impaired T_H1 and T_H17 differentiation.

Together, these results indicate that Satb1 deficiency limits T_H17 differentiation both *in vitro* and *in vivo*. In EAE and experimental colitis, Satb1 loss prevents disease by reducing the differentiation of both pathogenic and non-pathogenic $CD4^+$ T_H17 cells, leading to diminished expansion and inflammation. These findings highlight Satb1 as essential for T_H17-driven autoimmunity, acting during both the effector phase and early disease development.

Overexpression of Satb1 expression leads to increased T_H17 cell differentiation

Since Satb1 deletion impaired T_H17 generation, we next tested whether Satb1 overexpression enhances T_H17 differentiation.

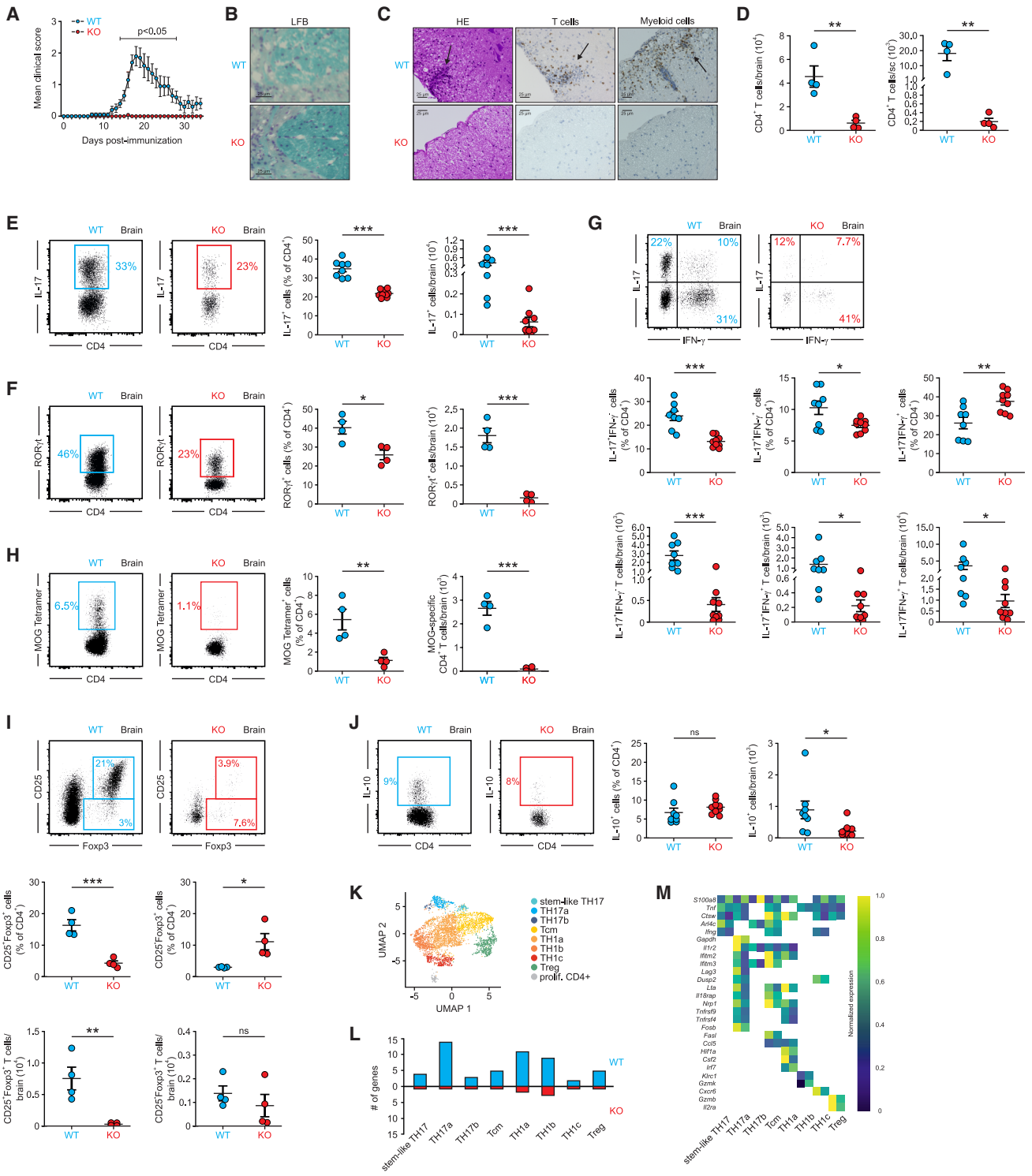

Figure 3. Loss of Satb1 prevents EAE development through decreased differentiation of T_H17 cells

Analysis of EAE development in Satb1$^{fl/fl}$ × CD4-CreERT2 mice at peak of disease.

(A) Mean EAE clinical score (WT *n* = 10, KO *n* = 12).

(B) Representative spinal cord myelin staining with luxol fast blue. Scale bar, 25 μm.

(C) Representative HE, anti-CD3, and anti-Mac3 staining of spinal cord sections. Scale bar, 25 μm.

(D) CD4$^+$ T cell counts in brain and spinal cord by flow cytometry (*n* = 4/group).

(legend continued on next page)

To this end, we created mice with conditional Satb1 overexpression by inserting the Satb1 coding sequence into the *Rosa26 locus* (Figure S5A). The construct includes a loxP-flanked stop cassette, followed by the *Satb1* sequence, an internal ribosome entry site (IRES), and *eGFP*, allowing overexpression to be tracked via eGFP after Cre-mediated recombination. A chicken actin promoter upstream of the stop cassette ensures ubiquitous expression post-recombination. Transgene integration was confirmed by PCR and Southern blot (Figures S5B and S5C). To elucidate the impact of Satb1 overexpression on naive $CD4^+$ T cell differentiation, we crossed conditional Satb1 knockin mice with CD4-Cre mice[43] to upregulate Satb1 in $CD4^+$ T cells. Cre recombination was confirmed via eGFP expression (Figure S5D), and Satb1 overexpression was validated at the mRNA and protein levels. As Satb1 is already abundant in naive but limited in effector/memory $CD4^+$ T cells (Figures S1A–S1C), the transgene had little impact on mRNA in naive cells (Figure S5E) but was detectable in effector/memory cells (Figure S5F) with no effect on T cell numbers or development. Nonetheless, Satb1 protein levels increased in both naive (Figure 4A) and effector/memory $CD4^+$ T cells (Figure 4B).

To assess whether elevated Satb1 affects T_H17 generation, we differentiated Satb1-overexpressing naive $CD4^+$ T cells *in vitro*. Satb1 overexpression led to a significant increase in IL-17^+ cells (Figure 4C) and elevated RORγt expression (Figure 4D). To evaluate effects on other T_H subsets, we performed additional differentiation assays. While T_H2 differentiation remained unchanged, T_H1 and iT_{reg} differentiation were reduced in Satb1-overexpressing cells (Figures S5G–S5K).

Next, we investigated the *in vivo* effect of Satb1 overexpression on T_H17 generation. Under homeostatic conditions, T_H17 cells reside in barrier organs to maintain tissue integrity.[44] In 27- to 30-week-old Satb1-WT and -overexpressing mice, we observed increased T_H17 cells in the small intestine (Figure 4E). Satb1-overexpressing animals also showed elevated IL-17^+ cells in non-barrier sites like mesLN (Figure 4F). Consistent with our previous observations, Satb1 overexpression expanded pathogenic IL-17^+IFN-γ^+ T_H17 cells in the small intestine (Figure 4G) and mesLN (Figure 4H). These findings demonstrate Satb1-dependent spontaneous T_H17 induction and underscore its role in T_H17 lineage commitment.

Loss of Satb1 alters chromatin accessibility and transcriptional networks

Since T_H17 generation is abolished when Satb1 is lost early during differentiation, we hypothesized that Satb1 promotes chromatin accessibility and gene-expression changes in naive $CD4^+$ T cells, critical for T_H17 fate.[20,28] We performed assay for transposase-accessible chromatin using sequencing (ATAC-seq) on Satb1-sufficient and Satb1-deficient naive $CD4^+$ T cells to compare chromatin accessibility (Figure S6A). While most regions were similar, Satb1-deficient cells showed 678 regions linked to nearby gene loci with increased and 116 with decreased accessibility (Figures 5A and S6B; Table S1), supporting the role of Satb1 in chromatin remodeling and gene silencing.[9] Differentially accessible regions (DARs) were enriched for genes involved in T cell activation, differentiation, and adhesion (Figure 5B).

To determine if increased chromatin accessibility results in changes in gene expression, we performed transcriptome analysis of Satb1-sufficient and Satb1-deficient naive $CD4^+$ T cells (Figures S6C and S6D). Despite a more open chromatin landscape in Satb1-deficient cells, only 116 genes were differentially expressed (DE) under homeostatic conditions (Figure 5C; Table S2). Linking ATAC-seq with gene-expression data revealed that a small subset of DARs corresponded to changes in gene expression, including *Il7r* and *Ifngr1* (Figures 5D and S6E). However, most accessible regions did not show transcriptional changes, suggesting that Satb1 deletion creates a pre-activated epigenetic state requiring additional signals for full gene activation.

To better understand how loss of Satb1 prevents T_H17 differentiation, we analyzed chromatin accessibility and gene expression at loci known to negatively regulate T_H17 cells (Figure 5E), finding minimal changes. This supports our earlier data (Figure 1D) that Satb1 does not broadly suppress negative regulators but influences T_H17 differentiation in a targeted manner. One key exception was *Il2*, which inhibits T_H17 differentiation.[45] In Satb1-deficient naive $CD4^+$ T cells, the *Il2* locus was accessible and *Il2* was already expressed at low levels (Figures 5D–5F and S6F). Functional annotation of DARs and DE genes indicated altered IL-2/Stat5 signaling in Satb1-deficient cells (Figures 5G, 5H, S6G, and S6H). These findings suggest Satb1 limits *Il2* expression to prevent premature activation and maintain naive $CD4^+$ T cell quiescence, thereby enabling proper T_H17 differentiation.

Satb1 allows for T_H17 cell differentiation by repressing IL-2 expression

As chromatin and transcriptome data indicated that Satb1 loss primes naive $CD4^+$ T cells for heightened activation and IL-2 signaling, we examined their response to TCR stimulation.

(E) $CD4^+$IL-17^+ T cells in the brain (WT $n = 8$, KO $n = 9$).
(F) $CD4^+$RORγt$^+$ T cells in the brain ($n = 4$/group).
(G) Non-pathogenic $CD4^+$IL-17^+IFN-γ^- T_H17, pathogenic $CD4^+$IL-17^+IFN-γ^+ T_H17 cells, and $CD4^+$IL-17^-IFN-γ^+ T_H1 cells in the brain (WT $n = 8$, KO $n = 9$).
(H) MOG-specific $CD4^+$ T cells in the brain ($n = 4$/group).
(I) $CD4^+Foxp3^+CD25^+$ T_{reg} cells and $CD4^+Foxp3^+CD25^-$ T cells in the brain ($n = 4$/group).
(J) IL-10-producing $CD4^+$ T cells in the brain (WT $n = 8$, KO $n = 9$).
(K) Uniform manifold approximation and projection (UMAP) clustering of CNS $CD4^+$ T cells.
(L) Differentially expressed gene (DEG) counts per cluster.
(M) Heatmap of DEGs in Satb1-sufficient (left) and -deficient (right) $CD4^+$ T cells.
(A and D–J) Data are shown as mean ± SEM. (A) Two-way repeated-measures ANOVA with Sidak's multiple comparison; (D–J) unpaired Student's t test (ns, not significant. $p \geq 0.05$; $^*p < 0.05$; $^{**}p < 0.01$; $^{***}p < 0.001$). (A and D) Data are representative of two independent experiments. (E–J) Data are pooled from two independent experiments. sc, spinal cord. See also Figure S4.

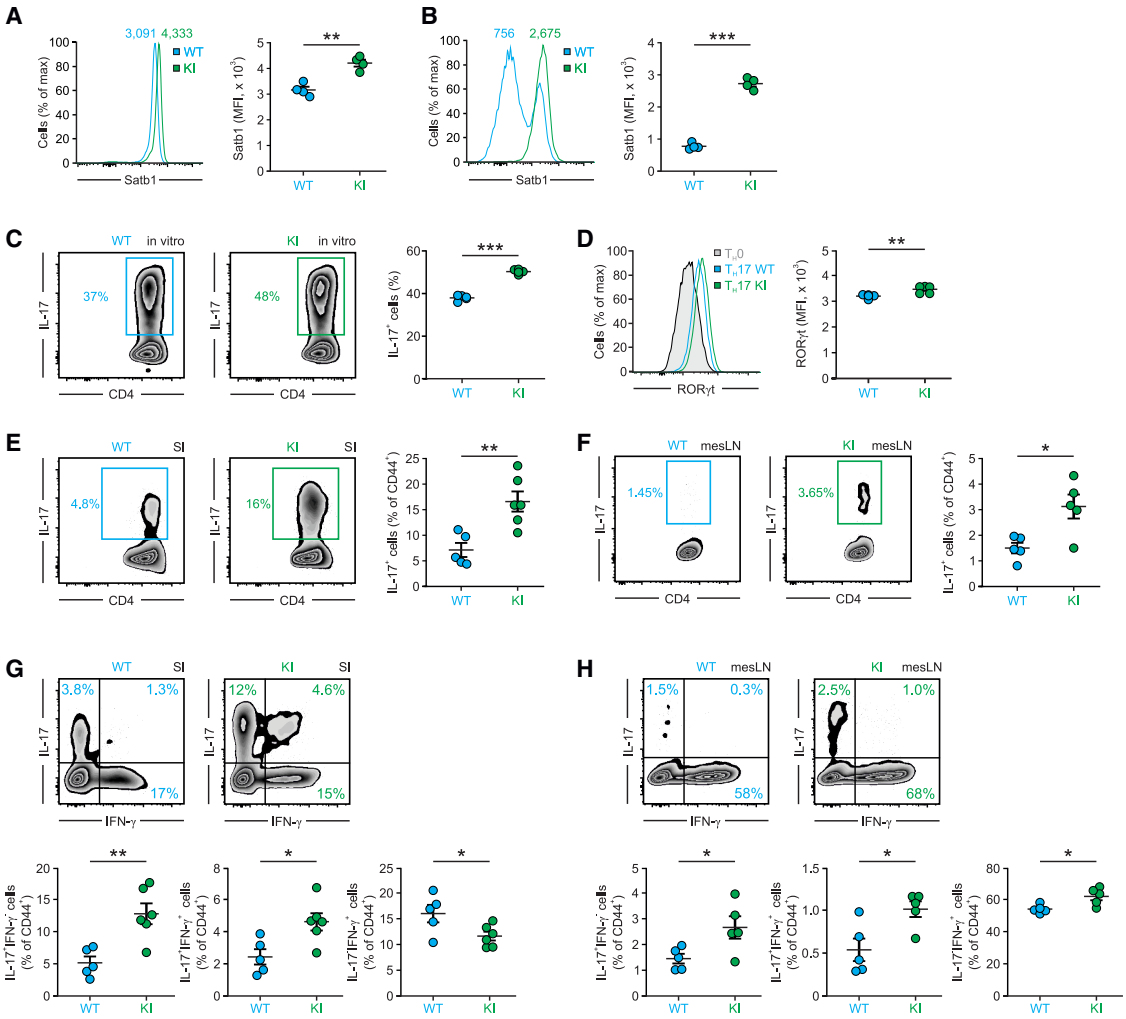

Figure 4. Overexpression of Satb1 improves T_H17 cell differentiation

Characterization of R26-STOP-Satb1$^{wt/+}$ × CD4-Cre$^{wt/wt}$ (WT) and R26-STOP-Satb1$^{wt/+}$ × CD4-Cre$^{wt/+}$ (KI) mice.

(A and B) Satb1 protein levels in (A) naive and (B) effector/memory CD4$^+$ T cells (n = 4/group).

(C and D) Satb1-WT and -overexpressing naive CD4$^+$ T cells were differentiated *in vitro* in T_H17 cells. Analysis of IL-17 (n = 5/group) (C) and RORγt (n = 5/group) (D) at day 5 of differentiation.

(E and F) IL-17 expression in effector/memory CD4$^+$ T cells from small intestine (WT n = 5, KI n = 6) (E) and mesLN in 27- to 30-week-old mice (WT n = 5, KI n = 5) (F).

(G and H) Non-pathogenic IL-17$^+$IFN-γ$^-$ T_H17, pathogenic IL-17$^+$IFN-γ$^+$ T_H17 cells, and IL-17$^-$IFN-γ$^+$ T_H1 cells within the effector/memory CD4$^+$ T cell pool of 27- to 30-week-old mice in the small intestine (WT n = 5, KI n = 6) (G) and mesLN (WT n = 5, KI n = 5) (H).

Data are shown as mean ± SEM. (A–H) Unpaired Student's t test (*p < 0.05, **p < 0.01, ***p < 0.001). (A and B) Data are representative of at least three independent experiments. (C) Data were pooled from two independent experiments. (D–H) Data are representative of two independent experiments. MFI, mean fluorescence intensity; mesLN, mesenteric lymph nodes. See also Figure S5.

Satb1-deficient cells showed elevated glycolytic activity (Figure 6A) and increased proliferation (Figure 6B), which supports the idea that a loss of Satb1 results in augmented CD4$^+$ T cell activation and proliferation and that loss of Satb1 is not directly linked to the reduced proliferation in both *in vivo* models. To exclude culture bias, we performed coculture experiments using Satb1-deficient and Satb1-sufficient CD4$^+$ T_{conv} cells, confirming increased proliferation of Satb1-deficient cells during T_H17 differentiation (Figures S7A–S7C). Consistently, *in vivo* bromodeoxyuridine (BrdU) incorporation and Ki-67 expression were elevated in Satb1-deficient naive CD4$^+$ T cells (Figures 6C and 6D), supporting the conclusion that their reduced proliferation in the EAE and colitis models reflects absence of inflammatory cues.

To further elucidate the role of IL-2, we analyzed IL-2 expression on mRNA as well as protein level. As indicated by increased chromatin accessibility, *Il2* mRNA was upregulated in Satb1-deficient naive CD4$^+$ T cells (Figure 6E). Correspondingly, IL-2 protein levels were elevated in spleen and mesLN CD4$^+$ T cells from Satb1$^{fl/fl}$ × CD4-CreERT2 mice 7 days after tamoxifen treatment (Figures 6F and S7D). This was confirmed in Satb1$^{fl/fl}$ × CD4-Cre mice, showing higher IL-2 production (Figure 6G). Both naive

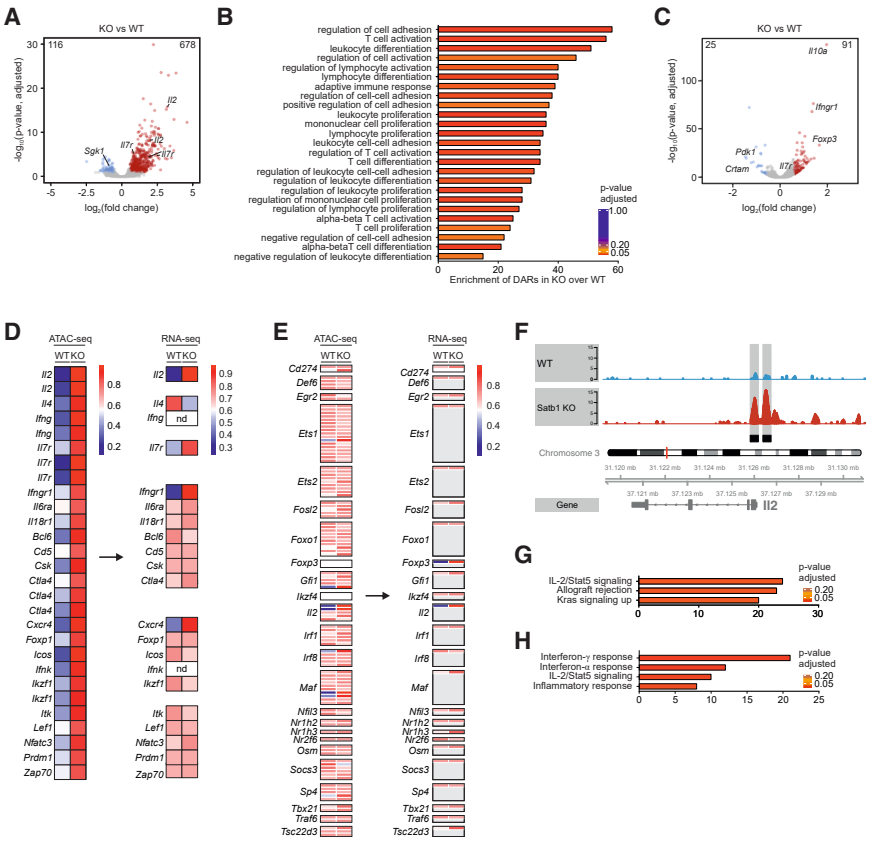

Figure 5. Satb1 retains the inactive state of naive CD4$^+$ T cells and blocks the accessibility of the *Il2* gene locus

ATAC-seq (n = 5/group) and RNA sequencing (n = 4/group) of naive CD4$^+$CD44$^-$CD62L$^+$CD25$^-$ T cells from Satb1$^{fl/fl}$ × CD4-CreERT2 mice.

(A) Volcano plot of differentially accessible regions (DARs).

(B) Gene Ontology (GO) analysis of DARs in Satb1-deficient cells.

(C) Volcano plot of differentially expressed genes (DEGs).

(D) Heatmap showing accessibility and expression of genes linked to T cell activation and differentiation.

(E) Heatmap of genes negatively regulating T_H17 differentiation.

(F) ATAC-seq profiles of the *Il2* locus.

(G) Enrichment of hallmark pathways (using MSigDB) in DARs accessible in Satb1-deficient cells.

(H) Enrichment of hallmark pathways (using MSigDB) in DEGs upregulated in Satb1-deficient cells.

(A, B, D, and G). Regions with an adjusted $p < 0.1$ and a fold change >1.5 were determined as significantly differentially accessible. (C and H) Genes with an adjusted $p < 0.05$ and a fold change >1.5 were determined as significantly DE. See also Figure S6.

and effector/memory CD4$^+$ T cells contributed to this increase (Figures S7E and S7F), and elevated IL-2 levels persisted up to 4 weeks post tamoxifen in Satb1-deficient CD4$^+$ T_{conv} cells isolated from the spleen of Satb1$^{fl/fl}$ × CD4-CreERT2 mice (Figure 6H). Similarly, high Ki-67 expression was maintained (left, Figure S7G). Caspase-3 levels were unchanged, ruling out reduced survival (right, Figure S7G), while Bcl-2 was elevated in Satb1-deficient cells (Figure S7H).

To determine if elevated IL-2 production is cell-intrinsic, we analyzed mice 4 weeks post tamoxifen, allowing thymic output of Satb1-sufficient naive CD4$^+$ T_{conv} cells. At 1 week, most peripheral CD4$^+$ T_{conv} cells were Satb1 deficient (GFP$^+$), but, by 4 weeks, a significant portion were Satb1 sufficient (GFP$^-$) (Figure S7I). As expected, GFP$^-$ Satb1-competent CD4$^+$ T_{conv} cells produced less IL-2 than their GFP$^+$ Satb1-deficient counterparts (Figure 6I).

We next administered a suboptimal tamoxifen dose to reduce *Satb1* recombination and utilized a competitive *in vivo* setting 1 week later (Figure S7J) to test for proliferative disadvantage of Satb1-deficient naive CD4$^+$ T cells. BrdU labeling and Ki-67 expression were increased in Satb1-deficient cells, indicating that Satb1 loss does not impair their proliferative capacity (Figures 6J and 6K).

As elevated IL-2 might promote T_{reg} development, we assessed T_{reg} frequencies in the spleen of Satb1$^{fl/fl}$ × CD4-CreERT2 mice 1 and 4 weeks post tamoxifen. While Foxp3$^+$ CD4$^+$ T cell percentages were increased at both time points (Figure S7K), most cells were CD25$^-$Foxp3^{low} (Figures S7L and S7M) and lacked typical T_{reg} markers (Figures S7N and S7O) while *bona fide* CD25$^+$Foxp3$^+$ T_{reg} cells remained unchanged. *In vitro*, iT_{reg} differentiation with low or no IL-2 yielded more Foxp3$^+$ Satb1-deficient cells, an effect fully blocked by anti-IL-2 and anti-CD25 antibodies (Figures S7P and S7Q). Conversely, Satb1 overexpression reduced IL-2 production in memory CD4$^+$ T cells (Figure S7R). These findings highlight the role of Satb1 in safeguarding CD4$^+$ T cell quiescence and proper differentiation by tightly regulating IL-2 expression via chromatin accessibility at the *Il2* locus.

To investigate whether Satb1 also regulates *Cd25*, as previously suggested,[9] we analyzed its expression in Satb1-deficient naive CD4$^+$ T cells. *Cd25* mRNA was upregulated (Figure S8A), but this was not reflected at the protein level (Figure S8B), supporting the idea that Satb1 loss primes naive T cells for activation, although full IL-2 signaling requires additional cues. As *Il2* is tightly regulated and repressed by factors like *Ets2* and *Pten* in naive and T_H17 cells,[46–48] we assessed their expression but observed no significant alterations in Satb1-deficient cells (Figure S8C). This suggests Satb1 represses *Il2* independently of Ets2 or Pten.

We next examined whether Satb1 deficiency impairs T_H17 differentiation via IL-2 signaling, which is known to inhibit T_H17 generation by modulating IL-6R expression and Stat5 activation.[49,50] Three days after T_H17 induction, Satb1-deficient cells showed slightly reduced IL-6Rα expression (Figure 6L) and increased Stat5 phosphorylation from 12 h onward (Figure 6M).

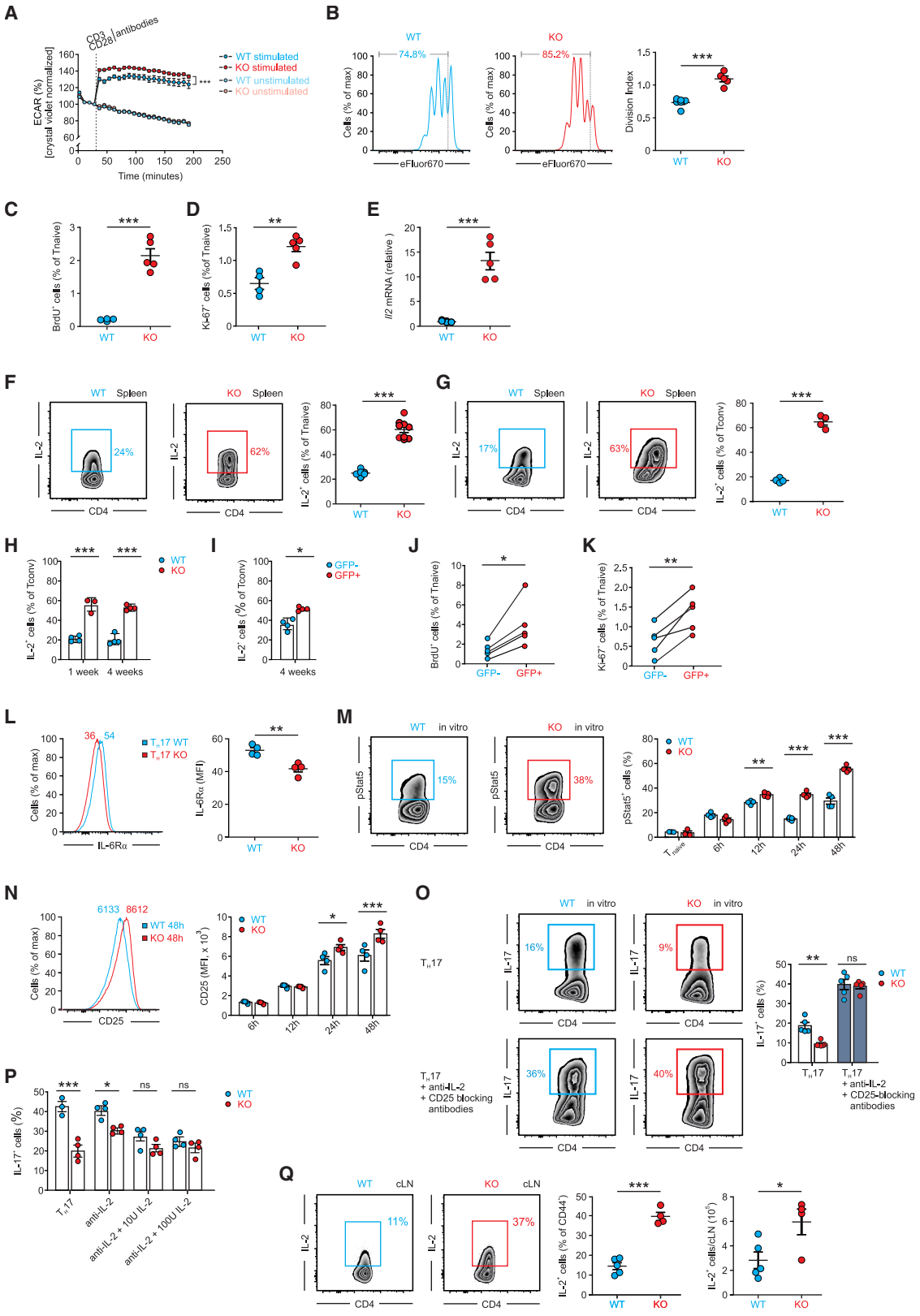

(legend on next page)

Correspondingly, CD25 was upregulated, reflecting enhanced IL-2/pStat5 signaling (Figure 6N). Since T_H17 differentiation depends on Stat3, and an altered Stat5:Stat3 balance can shift T_H17 fate, we analyzed Stat3 phosphorylation. Satb1-deficient cells had reduced pStat3, leading to an elevated pStat5:pStat3 ratio (Figures S8D and S8E). This shift supports the conclusion that increased Stat5 signaling suppresses the T_H17 gene program (Figure 1D).

To examine whether blocking IL-2/IL-2R signaling could rescue T_H17 differentiation in Satb1-deficient cells, we cultured $CD4^+$ T cells under T_H17 conditions with IL-2-neutralizing and CD25-blocking antibodies. Inhibition of IL-2 signaling restored IL-17 expression in Satb1-deficient cells to levels comparable with controls (Figure 6O). These results indicate that Satb1 promotes T_H17 differentiation primarily by limiting IL-2 signaling. To further validate the role of endogenous IL-2, we differentiated $CD4^+$ T cells into T_H17 cells with IL-2-neutralizing antibodies and increasing doses of human IL-2. IL-2 depletion partially restored T_H17 differentiation in Satb1-deficient cells, while human IL-2 reduced T_H17 differentiation in both Satb1-deficient and -sufficient cells (Figure 6P). In line with this, treatment with human IL-2 alone affected only T_H17 differentiation of Satb1-sufficient $CD4^+$ T cells as endogenously IL-2 produced by Satb1-deficient $CD4^+$ T cells is sufficient to prevent T_H17 differentiation (Figure S8F). Importantly, when Satb1-deficient and -sufficient $CD4^+$ T cells were cocultured, T_H17 differentiation improved in Satb1-deficient cells and slightly declined in Satb1-sufficient cells. This suggests that Satb1-sufficient cells consumed excess IL-2, lowering its availability and partially relieving IL-2-mediated inhibition in neighboring Satb1-deficient cells (Figure S8G).

To determine if IL-2 expression by naive $CD4^+$ T cells occurs *in vivo*, we induced EAE following Satb1 deletion. Upon stimulation, Satb1-deficient mice showed significantly more IL-2-producing naive $CD4^+$ T cells in cLN (Figure 6Q), spleen (Figure S8H), and mesLN (Figure S8I), reinforcing that Satb1 suppresses IL-2 expression to permit T_H17 differentiation.

Satb1 fine-tunes the differentiation potential of naive $CD4^+$ T cells

To evaluate the differentiation potential of Satb1-deficient naive $CD4^+$ T cells into T_H1 and T_H17 cells, we performed combined single-cell analysis of chromatin accessibility and mRNA expression (Figure 7A). Joint clustering of both data types showed that Satb1 loss does not alter T_{naive}, T_H1, or T_H17 identity but affects their differentiation extent (Figures 7B and S9A–S9C). In line with bulk data, Satb1-deficient naive $CD4^+$ T cells displayed increased accessibility at several immune-related loci, such as *Il7r*, *Ifng*, *Ifngr1*, *Ctla4*, and *Bcl2* (Figure 7C), with limited changes in corresponding gene expression (Figure 7D), yielding a Satb1-dependent signature of 45 genes (Figure 7E). As before, we could identify increased accessibility of the *Il2* locus in naive Satb1-deficient $CD4^+$ T cells (Figure 7F), while T_H1 and T_H17 cells showed reduced *Il2* accessibility and expression (Figure S9D). Enrichment analyses confirmed elevated IL-2/STAT5 signaling and STAT family transcription factor binding prediction in Satb1-deficient naive $CD4^+$ T cells (Figures 7G–7I). Analysis of DE genes and DARs between Satb1-deficient and -sufficient T_H1 and T_H17 cells revealed that loss of Satb1 is associated with a loss of differentiation potential of T_H17 cells (Figures 7J and 7K), while their T_H1 potential is increased (Figures 7L and 7M). This was further supported by functional annotation as loss of Satb1 resulted in enrichment of DARs and DE genes associated with IL-2/STAT5 signaling in T_H17 cells (Figures S9E and S9F) and T_H1 cells (Figures S9G and S9H), supporting the notion that Satb1 is affecting the differentiation of $CD4^+$ T cells by shaping the chromatin landscape for subsequent binding of transcription factors orchestrating $CD4^+$ T cell differentiation. The intersection of common DARs with associated genes regulated in T_H1 and T_H17 cells revealed a common set of genes associated with T cell differentiation and signaling (Figure 7N).

Taken together, our data support that Satb1 is important not only for fully committed T_H17 cells but also during their

Figure 6. Satb1 regulates T_H17 differentiation by controlling the expression of IL-2

(A and B) ECAR (A) and proliferation (B) of Satb1-sufficient (WT) and -deficient (KO) $CD4^+$ T cells from $Satb1^{fl/fl}$ × CD4-CreERT2 mice after CD3/CD28 stimulation (n = 10–13 for ECAR; WT n = 6, KO n = 5 for proliferation).

(C and D) BrdU incorporation (C) and Ki-67 expression (D) in) naive $CD4^+$ T cells from the spleen of $CD4^+CD25^-$ T_{conv} cells from $Satb1^{fl/fl}$ × CD4-CreERT2 mice (WT n = 4, KO n = 5).

(E and F) (E) *Il2* mRNA expression by RT-qPCR (n = 5/group) and (F) IL-2 protein expression in splenic $CD4^+CD44^-$ naive T cells from $Satb1^{fl/fl}$ × CD4-CreERT2 mice (WT n = 6, KO n = 5).

(G) IL-2 expression in splenic $CD4^+$ T cells of 44- to 60-week-old $Satb1^{fl/fl}$ × CD4-$Cre^{wt/wt}$ (WT) or $Satb1^{fl/fl}$ × CD4-$Cre^{wt/+}$ (KO) mice (n = 4/group).

(H) IL-2 expression in splenic $CD4^+CD44^-$ naive T cells from $Satb1^{fl/fl}$ × CD4-CreERT2 mice 1 week (left, WT n = 4, KO n = 3) or 4 weeks after tamoxifen administration (right, WT n = 4, KO n = 4).

(I) IL-2 expression in splenic Satb1-sufficient (GFP-) and Satb1-deficient (GFP+) $CD4^+CD44^-$ naive T cells from $Satb1^{fl/fl}$ × CD4-CreERT2 mice (WT n = 4, KO n = 4) 4 weeks after tamoxifen administration.

(J and K) BrdU incorporation (J) and Ki-67 expression (K) in splenic Satb1-sufficient (GFP-) and Satb1-deficient (GFP+) $CD4^+CD44^-$ naive T cells from $Satb1^{fl/fl}$ × CD4-CreERT2 mice (n = 5) 1 week after suboptimal tamoxifen administration.

(L–P) $CD4^+CD44^-CD62L^+CD25^-$ naive T cells from $Satb1^{fl/fl}$ × CD4-CreERT2 mice were isolated and differentiated *in vitro* into T_H17 cells. (L) IL-6Rα expression 3 days after initiation of differentiation (n = 4/group). (M) Stat5 phosphorylation at different time points during the differentiation (n = 3–4/group). (N) CD25 expression at different time points during the differentiation (n = 4/group). (O) IL-17 expression at day 5 of differentiation. Cells were cultured in absence or presence of anti-mouse IL-2 and CD25-blocking antibodies (n = 5/group). (P) IL-17 expression at day 3 of differentiation. Cells were cultured in the presence of anti-mouse IL-2 antibodies and 10 or 100 IU/mL human IL-2 (n = 4/group).

(Q) IL-2-producing $CD4^+CD44^-$ naive T cells in the cLN (WT n = 5, KO n = 4). Data are shown as mean ± SEM. (A) Two-way repeated-measures ANOVA with Tukey's multiple-comparison test; (B–I, L, and Q) unpaired Student's t test; (J and K) paired Student's t test; (M, N, and P) two-way ANOVA with Sidak's multiple-comparison test (ns, not significant; $p \geq 0.05$; *$p < 0.05$; **$p < 0.01$; ***$p < 0.001$). Data are representative of two independent experiments. cLN, cervical lymph node. See also Figures S7 and S8.

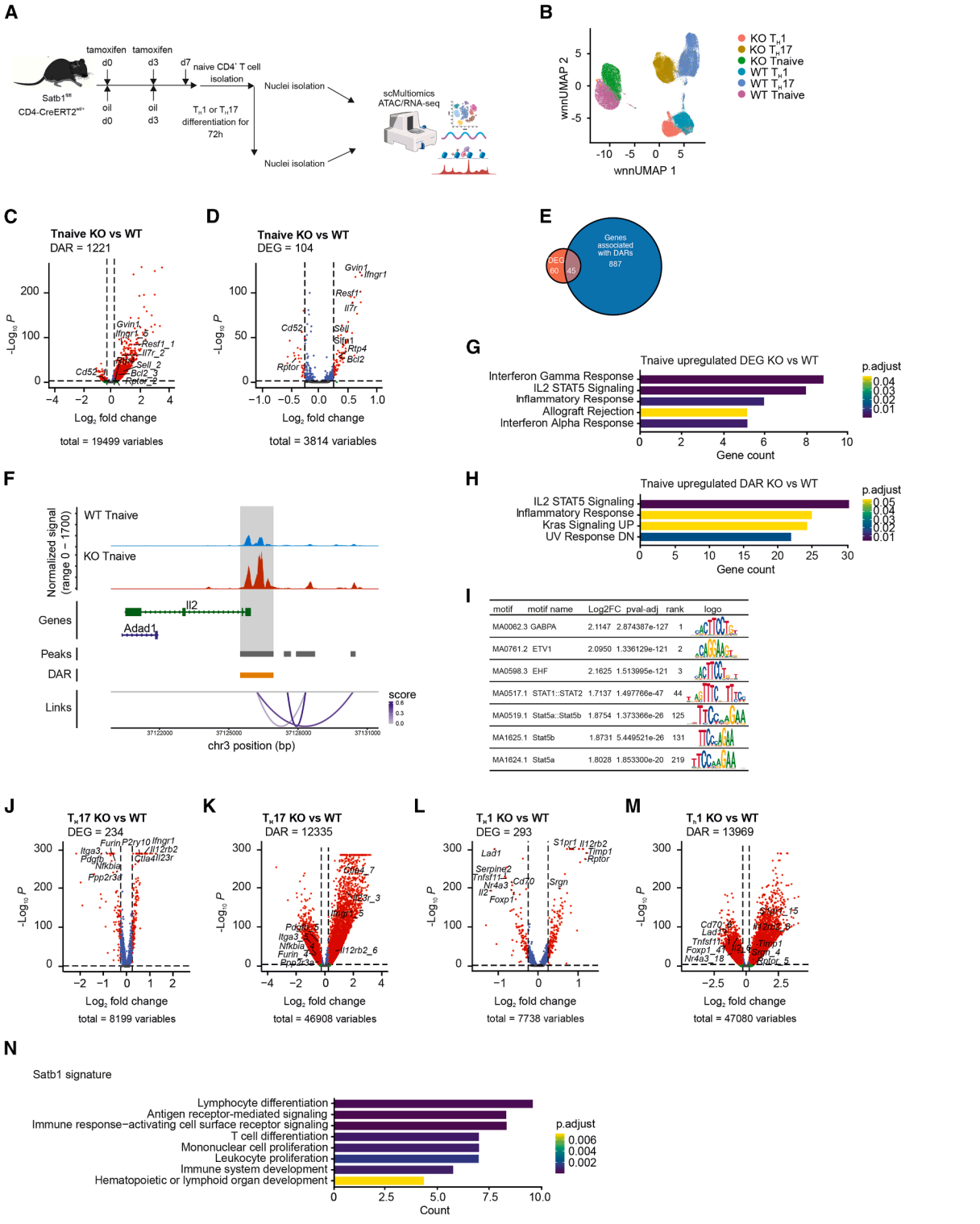

Figure 7. Satb1 expression in naive CD4$^+$ T cells orchestrates T_H1 and T_H17 cell differentiation by modifying chromatin accessibility and downstream gene expression

(A) Single-cell MultiOMICs workflow for naive CD4$^+$, T_H1, and T_H17 cells.

(B) UMAP projection showing genotype and cell type.

(C and D) Volcano plots of chromatin accessibility (C) and gene expression (D) in Satb1-deficient (KO) compared to Satb1-sufficient (WT) naive CD4$^+$ T cells.

(legend continued on next page)

differentiation through regulating the chromatin accessibility of the *Il2* gene locus and inhibiting IL-2 expression in naive $CD4^+$ T cells as well as in early stages of T_H17 differentiation. Based on this observation, we further substantiate the critical role of Satb1 in T_H17 cell biology and consequently T_H17-driven autoimmune diseases.

DISCUSSION

This study demonstrates that, beyond its role in T_H17 effector function, Satb1 is essential for initiating T_H17 differentiation. Satb1 is highly expressed in T_H17 cells, and its loss reduces, while its overexpression enhances, T_H17 development both *in vitro* and *in vivo*. We further show that Satb1 levels influence T_H17-driven diseases such as inflammatory bowel disease and EAE. Through chromatin accessibility and transcriptome analyses, we identify Satb1 as a key regulator of IL-2 expression in naive $CD4^+$ T cells. Our data provide strong evidence that Satb1 promotes T_H17 differentiation primarily by repressing IL-2, contrasting prior findings that linked loss of Satb1 during thymic development to reduced IL-2 expression.[26]

Bioinformatic predictions previously identified Satb1 as a potential regulator of T_H17 differentiation,[33,34] and small interfering RNA (siRNA) knockdown suggested a role in IL-17 expression.[33] Our functional analyses confirm and extend these findings, demonstrating that Satb1 is essential for T_H17 differentiation both *in vitro* and *in vivo*. Satb1 acts early, functioning as a pioneering factor that shapes the epigenetic landscape during T_H17 lineage commitment. While transcriptional master regulators define T_H subtypes, lineage stability depends on broader transcriptional networks.[33,51] Pioneering factors like Satb1 help establish these networks, and epigenetic regulation adds a crucial layer of control.[52,53] Interestingly, deletion of Satb1 in naive $CD4^+$ T cells impaired induction of the T_H17 gene program and GM-CSF production, with key T_H17-associated gene modules remaining unexpressed.[33,34] Consequently, T_H17 effector cytokines were nearly absent, explaining the complete protection from EAE even when Satb1 was deleted during the effector phase using a tamoxifen-inducible model.[7] Satb1 deletion also prevented colitis in the adoptive transfer model, underscoring its role in T_H17-driven diseases. The failure to induce T_H17 differentiation blocked inflammation-driven proliferation and reduced $IL\text{-}17^-IFN\text{-}\gamma^+$ $CD4^+$ T cells, indicating that increased T_H1 responses were also suppressed. By specifically deleting Satb1 in peripheral naive $CD4^+$ T cells and using the colitis model, we demonstrate that the function of Satb1 in T_H17 differentiation and disease development is cell intrinsic.

To date, only a few targets have been shown to fully prevent EAE. Disruption of T_H17 master regulators such as RORγt, Batf, Stat3, or the absence of IL-6 blocks disease development.[54–57] Similarly, deleting factors controlling T_H17 pathogenicity, including IL-23R, T-bet, and Gpr65, also prevents EAE.[4,58–60] We now identify Satb1 as an additional master regulator whose deletion inhibits EAE. Notably, disease outcome depends on the timing of Satb1 loss: deletion in naive $CD4^+$ T cells confers full resistance, while deletion in committed T_H17 cells only reduces disease severity.[7,8] This highlights Satb1's dual role in both T_H17 differentiation and effector function.

In humans, Satb1 has been linked to T_H17-driven diseases like multiple sclerosis,[61] and its overexpression in anaplastic T cell lymphoma is associated with a heightened T_H17 profile.[62] Thus, Satb1 or its downstream pathways may represent therapeutic targets for conditions involving excessive T_H17 responses, as its inhibition could impact both differentiation and pathogenic function. To investigate the role of Satb1 in T_H17 development, we compared Satb1-sufficient and -deficient naive $CD4^+$ T cells at the epigenetic and transcriptional levels. Satb1-deficient cells exhibited increased chromatin accessibility at several immune-related loci such as *Il7r* and *Ctla4*. Functional annotation suggests Satb1 helps to maintain naive $CD4^+$ T cells in a resting state, while its loss shifts cells toward a pre-activated phenotype.

Earlier findings described Satb1 predominately as a transcriptional repressor.[9] While its loss did not trigger widespread activation of T cell activation genes, epigenetic analysis suggests that Satb1-deficient cells acquire a permissive chromatin state, predisposing them to faster and stronger activation. However, additional activators are still required to drive gene expression. Consistently, Satb1-deficient cells showed enhanced responses to TCR stimulation, including increased glycolysis. Among the loci with increased accessibility was *Il2*, a known Satb1 target.[63,64] This led to elevated IL-2 expression upon short-term activation of naive $CD4^+$ T cells. This contrasts with a previous report showing reduced IL-2 and CD25 in Satb1-deficient $CD4^+$ T cells using CD4-Cre mice.[26] In our study, CD3/CD28 stimulation promoted proliferation of Satb1-deficient cells, indicating functional IL-2 signaling. Conversely, Satb1 overexpression reduced IL-2 in effector/memory T cells. Notably, scMultiOMICs revealed decreased *Il2* accessibility and mRNA in Satb1-deficient T_H1 and T_H17 cells, aligning with observations from total $CD4^+$ T cells after *in vitro* stimulation.[26]

IL-2 is a central regulator of both T_{reg} and T_H subset differentiation.[46,65] In T_{reg} cells, Satb1 acts as a pioneering factor for chromatin remodeling and Foxp3 induction.[20] While IL-2 supports T_{reg} survival, increased IL-2 in Satb1-deficient $CD4^+$

(E) Venn diagram of overlapping DEGs and DARs in naive $CD4^+$ T cells.
(F) ATAC-seq tracks and Cicero co-accessibility links for the *Il2* locus in naive $CD4^+$ T cells. The height of connections reflects the strength of Cicero co-accessibility scores between linked peaks.
(G) Hallmark pathway enrichment (MSigDB) in genes upregulated in KO naive $CD4^+$ T cells.
(H) Hallmark pathway enrichment (MSigDB) in regions more accessible in KO naive $CD4^+$ T cells.
(I) Transcription factor motif enrichment in DARs of KO naive $CD4^+$ T cells.
(J and K) Volcano plots of gene expression (J) and chromatin accessibility (K) in T_H17 cells.
(L and M) Volcano plots of gene expression (L) and chromatin accessibility (M) in T_H1 cells.
(N) Enrichment of GO terms in the intersection of the union of upregulated DEG genes from T_H1 and T_H17 cells associated with increased accessibility in naive $CD4^+$ T cells as well as T_H1 and T_H17 cells. See also Figure S9.

T cells did not enhance T_{reg} differentiation. Instead, we observed Foxp3^{low} CD4$^+$ T cells lacking canonical T_{reg} markers, suggesting activation rather than true T_{reg} development. This implies that, while Satb1 loss may favor a T_{reg}-permissive state, additional signals like TGF-β are needed for full differentiation. IL-2 also inhibits T_H17 differentiation,[46,65] and Pten is known to repress *Il2* during this process.[47] Satb1 deficiency produced an even stronger phenotype, supporting its role in promoting T_H17 differentiation by repressing *Il2*. Furthermore, both IL-6Rα expression and Stat5 activation were altered in Satb1-deficient cells under T_H17-polarizing conditions, with elevated Stat5 phosphorylation. The balance between Stat3 and Stat5 activation is known to regulate epigenetic remodeling and gene transcription,[50,66] and its disruption impairs T_H17 differentiation.[50] In Satb1-deficient cells, increased CD25 expression indicated enhanced pStat5 signaling, while IL-6Rα and IL-17, normally induced by pStat3 but repressed by IL-2/pStat5,[67] were reduced. Thus, Satb1-deficient cells showed decreased Stat3 and increased Stat5 signaling during T_H17 differentiation. Blocking IL-2/IL-2R signaling in Satb1-deficient CD4$^+$ T cells restored T_H17 differentiation and partially rescued features like GM-CSF production (data not shown), confirming that Satb1 promotes T_H17 development by repressing IL-2 and limiting Stat5 activation.

All together, we identified that Satb1 is important in the early phase of the development of T_H17 cells by repressing the accessibility of the *Il2* locus preventing IL-2 expression, subsequent IL-2R signaling, and Stat5 phosphorylation. Consequently, Satb1 is required for the preservation of pStat3 signaling and the establishment of the T_H17-specific gene network allowing for T_H17 differentiation and T_H17-driven disease formation. Hence, Satb1 is required not only for pathogenic T_H17 function but also for the initiation of T_H17 differentiation and can be defined as a new T_H17 pioneering factor.

Limitations of the study

While our study reveals how Satb1 deletion prevents T_H17-mediated autoimmunity via IL-2/STAT5 signaling, it is based on a conditional mouse model, which may not fully capture the complexity of human immune responses. We also note differences from previous T cell-specific Satb1 KO models, highlighting variability across systems. Species-specific differences may limit the direct translation of our findings, underscoring the need to validate them in human T_H17 cells. Advances in CRISPR-Cas9 gene editing and human lymphoid organoid models now offer promising tools to study gene function in more physiologically relevant human settings.

RESOURCE AVAILABILITY

Lead contact

Further information and requests for resources and reagents should be directed to and will be fulfilled by the lead contact, PD Dr. Marc D. Beyer (marc.beyer@dzne.de).

Materials availability

This study did not generate new unique reagents.

Data and code availability

The accession numbers for the sequencing data are as follows: super-series GSE250579 (bulk RNA sequencing, GSE250577; scRNA-seq resp. scMultiOMICs, GSE250578, GSE290258; ATAC-seq, GSE250576). All code is available at https://gitlab.dzne.de/ag-beyer/KoehneShakiba_Satb1 for reproducibility and further analysis (https://doi.org/10.5281/zenodo.15201055). Any additional information required to reanalyze the data reported in this paper is available from the lead contact upon request.

ACKNOWLEDGMENTS

We thank Michael Kraut, Heidi Theis, Stephanie Weber, Dina Huesson, and Maren Schnell for technical assistance; Heike Weighardt for critical discussions; and the LIMES-GRC for the generation of mice. MOG_{38-49}/I-Ab tetramer and unloaded control tetramer were kindly provided by the NIH tetramer core facility. M.D.B. is supported by the Helmholtz Association and the German Research Foundation (DFG) (BE4427/3-1, 269749094; SFB1454, 432325352; IGK2168/2, 272482170). M.D.B., L.B., M.G., and J.L.S. are members of the excellence cluster ImmunoSensation2 (EXC2151, 390873048). J.L.S. is funded by the BMBF (DietBB, 01EA1809A; iTREAT, 01ZX1902A). L.B. is funded by the DFG (ImmuDiet, 513977171) and the European Research Council (ERC) under the European Union's Horizon 2020 research and innovation program (101163024, POLIS). M.G. is supported by the ERC Advanced Grant NalpACT. D.H. received a stipend from the Schlumberger Foundation Faculty of the Future. J.A. has been funded by DFG (EXC 1003, FF-2014-01, Cells in Motion; FOR2107, AL1145/5-2; SFB/TRR393 A05, 521379614). T.B. is funded by the Swiss National Science Foundation (SNF, 310030-197652 and 310030-116201).

AUTHOR CONTRIBUTIONS

Conceptualization, M.K. and M.D.B.; investigation, data curation, and formal analysis, M.K., M.H.S., L.S., D.S., J.S.-S., T.E., R.S., L.B., Y.L., E.D.D., J.W., K.H., A.F., X.C., C.O.-S., S.B., L.H., Y.T., H.R., D.H., C.C., S.P., A.-K.B., C. W., J.A., and T.K.; resources and methodology, T.S., T.B., F.T.W., M.G., S. C.B., J.A., and M.D.B.; visualization, M.K., M.H.S., J.S.-S., R.S., and M.D.B.; funding acquisition, J.L.S. and M.D.B.; supervision, M.K., J.L.-S., and M.D. B.; writing – original draft & revision, M.K., M.H.S., and M.D.B.; writing – review & editing, all authors.

DECLARATION OF INTERESTS

The authors declare no competing interests.

STAR★METHODS

Detailed methods are provided in the online version of this paper and include the following:

- KEY RESOURCES TABLE
- EXPERIMENTAL MODEL AND STUDY PARTICIPANT DETAILS
  - Mice
  - Primary cells and cell lines
  - Microbe strains
- METHOD DETAILS
  - Generation of Satb1-overexpressing mice
  - Tamoxifen administration
  - Induction and assessment of experimental colitis
  - Induction of experimental autoimmune encephalomyelitis (EAE)
  - Isolation of immune cells
  - Isolation of naive and effector/memory CD4$^+$ T cells
  - *In vitro* CD4$^+$ T cell differentiation
  - Proliferation assays
  - Labeling of CD4$^+$ T cells with PKH26 or eFluor670 for co-culture experiments
  - *In vivo* BrdU labeling of T cells and anti-BrdU staining to assess cell proliferation

- Analysis of metabolic parameters
- Antibodies, staining and flow cytometry analysis
- Immunoblot analysis for Satb1
- Histology
- Quantitative RT-PCR
- Transcriptome analysis of naive $CD4^+$ T cells
- Analysis of Satb1 dependence on RORγt and Stat3
- Single-cell RNA-seq of $CD4^+$ T cells in EAE
- Assay for Transposase accessible chromatin (ATAC)-Sequencing of naive $CD4^+$ T cells
- Single-cell ATAC-seq and whole transcriptome analysis of naive $CD4^+$ T cells and *in vitro* differentiated T_H1 and T_H17 cells

- QUANTIFICATION AND STATISTICAL ANALYSIS

SUPPLEMENTAL INFORMATION

Supplemental information can be found online at https://doi.org/10.1016/j.celrep.2025.115866.

Received: January 16, 2024
Revised: March 14, 2025
Accepted: May 28, 2025

REFERENCES

1. Korn, T., Bettelli, E., Oukka, M., and Kuchroo, V.K. (2009). IL-17 and Th17 Cells. Annu. Rev. Immunol. *27*, 485–517. https://doi.org/10.1146/annurev.immunol.021908.132710.
2. Yamada, H. (2010). Current perspectives on the role of IL-17 in autoimmune disease. J. Inflamm. Res. *3*, 33–44. https://doi.org/10.2147/jir.s6375.
3. Zambrano-Zaragoza, J.F., Romo-Martínez, E.J., Durán-Avelar, M.d.J., García-Magallanes, N., and Vibanco-Pérez, N. (2014). Th17 Cells in Autoimmune and Infectious Diseases. Int. J. Inflam. *2014*, 651503. https://doi.org/10.1155/2014/651503.
4. Gaublomme, J.T., Yosef, N., Lee, Y., Gertner, R.S., Yang, L.V., Wu, C., Pandolfi, P.P., Mak, T., Satija, R., Shalek, A.K., et al. (2015). Single-Cell Genomics Unveils Critical Regulators of Th17 Cell Pathogenicity. Cell *163*, 1400–1412. https://doi.org/10.1016/j.cell.2015.11.009.
5. Langrish, C.L., Chen, Y., Blumenschein, W.M., Mattson, J., Basham, B., Sedgwick, J.D., McClanahan, T., Kastelein, R.A., and Cua, D.J. (2005). IL-23 drives a pathogenic T cell population that induces autoimmune inflammation. J. Exp. Med. *201*, 233–240. https://doi.org/10.1084/jem.20041257.
6. Lee, Y., Awasthi, A., Yosef, N., Quintana, F.J., Xiao, S., Peters, A., Wu, C., Kleinewietfeld, M., Kunder, S., Hafler, D.A., et al. (2012). Induction and molecular signature of pathogenic TH17 cells. Nat. Immunol. *13*, 991–999. https://doi.org/10.1038/ni.2416.
7. Akiba, Y., Kuwabara, T., Mukozu, T., Mikami, T., and Kondo, M. (2018). Special AT-rich sequence binding protein 1 is required for maintenance of T cell receptor responsiveness and development of experimental autoimmune encephalomyelitis. Microbiol. Immunol. *62*, 255–268. https://doi.org/10.1111/1348-0421.12579.
8. Yasuda, K., Kitagawa, Y., Kawakami, R., Isaka, Y., Watanabe, H., Kondoh, G., Kohwi-Shigematsu, T., Sakaguchi, S., and Hirota, K. (2019). Satb1 regulates the effector program of encephalitogenic tissue Th17 cells in chronic inflammation. Nat. Commun. *10*, 549. https://doi.org/10.1038/s41467-019-08404-w.
9. Alvarez, J.D., Yasui, D.H., Niida, H., Joh, T., Loh, D.Y., and Kohwi-Shigematsu, T. (2000). The MAR-binding protein SATB1 orchestrates temporal and spatial expression of multiple genes during T-cell development. Genes Dev. *14*, 521–535.
10. Cai, S., Han, H.-J., and Kohwi-Shigematsu, T. (2003). Tissue-specific nuclear architecture and gene expression regulated by SATB1. Nat. Genet. *34*, 42–51. https://doi.org/10.1038/ng1146.
11. Gong, F., Sun, L., Wang, Z., Shi, J., Li, W., Wang, S., Han, X., and Sun, Y. (2011). The BCL2 gene is regulated by a special AT-rich sequence binding protein 1-mediated long range chromosomal interaction between the promoter and the distal element located within the 3′-UTR. Nucleic Acids Res. *39*, 4640–4652. https://doi.org/10.1093/nar/gkr023.
12. Yang, Y., Wang, Z., Sun, L., Shao, L., Yang, N., Yu, D., Zhang, X., Han, X., and Sun, Y. (2015). SATB1 mediates long-range chromatin interactions: A dual regulator of anti-apoptotic BCL2 and pro-apoptotic NOXA genes. PLoS One *10*, e0139170. https://doi.org/10.1371/journal.pone.0139170.
13. Wang, B., Ji, L., and Bian, Q. (2023). SATB1 regulates 3D genome architecture in T cells by constraining chromatin interactions surrounding CTCF-binding sites. Cell Rep. *42*, 112323. https://doi.org/10.1016/j.celrep.2023.112323.
14. Zelenka, T., Klonizakis, A., Tsoukatou, D., Papamatheakis, D.A., Franzenburg, S., Tzerpos, P., Tzonevrakis, I.R., Papadogkonas, G., Kapsetaki, M., Nikolaou, C., et al. (2022). The 3D enhancer network of the developing T cell genome is shaped by SATB1. Nat. Commun. *13*, 6954. https://doi.org/10.1038/s41467-022-34345-y.
15. Yasui, D., Miyano, M., Cai, S., Varga-Weisz, P., and Kohwi-Shigematsu, T. (2002). SATB1 targets chromatin remodelling to regulate genes over long distances. Nature *419*, 641–645. https://doi.org/10.1038/nature01084.
16. Doi, Y., Yokota, T., Satoh, Y., Okuzaki, D., Tokunaga, M., Ishibashi, T., Sudo, T., Ueda, T., Shingai, Y., Ichii, M., et al. (2018). Variable SATB1 Levels Regulate Hematopoietic Stem Cell Heterogeneity with Distinct Lineage Fate. Cell Rep. *23*, 3223–3235. https://doi.org/10.1016/j.celrep.2018.05.042.
17. Gottimukkala, K.P., Jangid, R., Patta, I., Sultana, D.A., Sharma, A., Misra-Sen, J., and Galande, S. (2016). Regulation of SATB1 during thymocyte development by TCR signaling. Mol. Immunol. *77*, 34–43. https://doi.org/10.1016/j.molimm.2016.07.005.
18. Hao, B., Naik, A.K., Watanabe, A., Tanaka, H., Chen, L., Richards, H.W., Kondo, M., Taniuchi, I., Kohwi, Y., Kohwi-Shigematsu, T., and Krangel, M.S. (2015). An anti-silencer– and SATB1-dependent chromatin hub regulates Rag1 and Rag2 gene expression during thymocyte development. J. Exp. Med. *212*, 809–824. https://doi.org/10.1084/jem.20142207.
19. Kakugawa, K., Kojo, S., Tanaka, H., Seo, W., Endo, T.A., Kitagawa, Y., Muroi, S., Tenno, M., Yasmin, N., Kohwi, Y., et al. (2017). Essential Roles of SATB1 in Specifying T Lymphocyte Subsets. Cell Rep. *19*, 1176–1188. https://doi.org/10.1016/j.celrep.2017.04.038.
20. Kitagawa, Y., Ohkura, N., Kidani, Y., Vandenbon, A., Hirota, K., Kawakami, R., Yasuda, K., Motooka, D., Nakamura, S., Kondo, M., et al. (2017). Guidance of regulatory T cell development by Satb1-dependent super-enhancer establishment. Nat. Immunol. *18*, 173–183. https://doi.org/10.1038/ni.3646.
21. Kondo, M., Tanaka, Y., Kuwabara, T., Naito, T., Kohwi-Shigematsu, T., and Watanabe, A. (2016). SATB1 Plays a Critical Role in Establishment of Immune Tolerance. J. Immunol. *196*, 563–572. https://doi.org/10.4049/jimmunol.1501429.
22. Nie, H., Maika, S.D., Tucker, P.W., and Gottlieb, P.D. (2005). A Role for SATB1, a Nuclear Matrix Association Region-Binding Protein, in the Development of CD8SP Thymocytes and Peripheral T Lymphocytes. J. Immunol. *174*, 4745–4752. https://doi.org/10.4049/jimmunol.174.8.4745.
23. Satoh, Y., Yokota, T., Sudo, T., Kondo, M., Lai, A., Kincade, P.W., Kouro, T., Iida, R., Kokame, K., Miyata, T., et al. (2013). The Satb1 Protein Directs Hematopoietic Stem Cell Differentiation toward Lymphoid Lineages. Immunity *38*, 1105–1115. https://doi.org/10.1016/j.immuni.2013.05.014.
24. Feng, D., Chen, Y., Dai, R., Bian, S., Xue, W., Zhu, Y., Li, Z., Yang, Y., Zhang, Y., Zhang, J., et al. (2022). Chromatin organizer SATB1 controls the cell identity of CD4(+) CD8(+) double-positive thymocytes by

regulating the activity of super-enhancers. Nat. Commun. *13*, 5554. https://doi.org/10.1038/s41467-022-33333-6.

25. Feng, D., Li, Z., Qin, L., and Hao, B. (2021). The role of chromatin organizer Satb1 in shaping TCR repertoire in adult thymus. Genome *64*, 821–832. https://doi.org/10.1139/gen-2020-0139.
26. Gupta, P.K., Allocco, J.B., Fraipont, J.M., McKeague, M.L., Wang, P., Andrade, M.S., McIntosh, C., Chen, L., Wang, Y., Li, Y., et al. (2022). Reduced Satb1 expression predisposes CD4(+) T conventional cells to Treg suppression and promotes transplant survival. Proc. Natl. Acad. Sci. USA *119*, e2205062119. https://doi.org/10.1073/pnas.2205062119.
27. Ahlfors, H., Limaye, A., Elo, L.L., Tuomela, S., Burute, M., Gottimukkala, K.V.P., Notani, D., Rasool, O., Galande, S., and Lahesmaa, R. (2010). SATB1 dictates expression of multiple genes including IL-5 involved in human T helper cell differentiation. Blood *116*, 1443–1453. https://doi.org/10.1182/blood-2009-11-252205.
28. Cai, S., Lee, C.C., and Kohwi-Shigematsu, T. (2006). SATB1 packages densely looped, transcriptionally active chromatin for coordinated expression of cytokine genes. Nat. Genet. *38*, 1278–1288. https://doi.org/10.1038/ng1913.
29. Notani, D., Gottimukkala, K.P., Jayani, R.S., Limaye, A.S., Damle, M.V., Mehta, S., Purbey, P.K., Joseph, J., and Galande, S. (2010). Global Regulator SATB1 Recruits β-Catenin and Regulates TH2 Differentiation in Wnt-Dependent Manner. PLoS Biol. *8*, e1000296. https://doi.org/10.1371/journal.pbio.1000296.
30. Chaurio, R.A., Anadon, C.M., Lee Costich, T., Payne, K.K., Biswas, S., Harro, C.M., Moran, C., Ortiz, A.C., Cortina, C., Rigolizzo, K.E., et al. (2022). TGF-beta-mediated silencing of genomic organizer SATB1 promotes Tfh cell differentiation and formation of intra-tumoral tertiary lymphoid structures. Immunity *55*, 115–128.e9. https://doi.org/10.1016/j.immuni.2021.12.007.
31. Beyer, M., Thabet, Y., Müller, R.-U., Sadlon, T., Classen, S., Lahl, K., Basu, S., Zhou, X., Bailey-Bucktrout, S.L., Krebs, W., et al. (2011). Repression of the genome organizer SATB1 in regulatory T cells is required for suppressive function and inhibition of effector differentiation. Nat. Immunol. *12*, 898–907. https://doi.org/10.1038/ni.2084.
32. Li, Y., Wang, J., Yu, M., Wang, Y., Zhang, H., Yin, J., Li, Z., Li, T., Yan, H., Li, F., and Wang, X. (2018). SNF5 deficiency induces apoptosis resistance by repressing SATB1 expression in Sézary syndrome. Leuk. Lymphoma *59*, 2405–2413. https://doi.org/10.1080/10428194.2017.1422861.
33. Ciofani, M., Madar, A., Galan, C., Sellars, M., Mace, K., Pauli, F., Agarwal, A., Huang, W., Parkhurst, C.N., Muratet, M., et al. (2012). A Validated Regulatory Network for Th17 Cell Specification. Cell *151*, 289–303. https://doi.org/10.1016/j.cell.2012.09.016.
34. Yosef, N., Shalek, A.K., Gaublomme, J.T., Jin, H., Lee, Y., Awasthi, A., Wu, C., Karwacz, K., Xiao, S., Jorgolli, M., et al. (2013). Dynamic regulatory network controlling TH17 cell differentiation. Nature *496*, 461–468. https://doi.org/10.1038/nature11981.
35. Sommer, D., Peters, A., Wirtz, T., Mai, M., Ackermann, J., Thabet, Y., Schmidt, J., Weighardt, H., Wunderlich, F.T., Degen, J., et al. (2014). Efficient genome engineering by targeted homologous recombination in mouse embryos using transcription activator-like effector nucleases. Nat. Commun. *5*, 3045. https://doi.org/10.1038/ncomms4045.
36. Śledzińska, A., Hemmers, S., Mair, F., Gorka, O., Ruland, J., Fairbairn, L., Nissler, A., Müller, W., Waisman, A., Becher, B., and Buch, T. (2013). TGF-β Signalling Is Required for CD4+ T Cell Homeostasis But Dispensable for Regulatory T Cell Function. PLoS Biol. *11*, e1001674. https://doi.org/10.1371/journal.pbio.1001674.
37. Stephen, T.L., Payne, K.K., Chaurio, R.A., Allegrezza, M.J., Zhu, H., Perez-Sanz, J., Perales-Puchalt, A., Nguyen, J.M., Vara-Ailor, A.E., Eruslanov, E.B., et al. (2017). SATB1 Expression Governs Epigenetic Repression of PD-1 in Tumor-Reactive T Cells. Immunity *46*, 51–64. https://doi.org/10.1016/j.immuni.2016.12.015.
38. Ahern, P.P., Schiering, C., Buonocore, S., McGeachy, M.J., Cua, D.J., Maloy, K.J., and Powrie, F. (2010). Interleukin-23 Drives Intestinal Inflammation through Direct Activity on T Cells. Immunity *33*, 279–288. https://doi.org/10.1016/j.immuni.2010.08.010.
39. Leppkes, M., Becker, C., Ivanov, I.I., Hirth, S., Wirtz, S., Neufert, C., Pouly, S., Murphy, A.J., Valenzuela, D.M., Yancopoulos, G.D., et al. (2009). RORγ-Expressing Th17 Cells Induce Murine Chronic Intestinal Inflammation via Redundant Effects of IL-17A and IL-17F. Gastroenterology (New York, N. Y., 1943) *136*, 257–267. https://doi.org/10.1053/j.gastro.2008.10.018.
40. Yen, D., Cheung, J., Scheerens, H., Poulet, F., McClanahan, T., McKenzie, B., Kleinschek, M.A., Owyang, A., Mattson, J., Blumenschein, W., et al. (2006). IL-23 is essential for T cell–mediated colitis and promotes inflammation via IL-17 and IL-6. J. Clin. Investig. *116*, 1310–1316. https://doi.org/10.1172/JCI21404.
41. Powrie, F., Leach, M.W., Mauze, S., Caddle, L.B., and Coffman, R.L. (1993). Phenotypically distinct subsets of CD4+ T cells induce or protect from chronic intestinal inflammation in C. B-17 scid mice. Int. Immunol. *5*, 1461–1471. https://doi.org/10.1093/intimm/5.11.1461.
42. Duhen, R., Glatigny, S., Arbelaez, C.A., Blair, T.C., Oukka, M., and Bettelli, E. (2013). Cutting edge: the pathogenicity of IFN-γ-producing Th17 cells is independent of T-bet. J. Immunol. *190*, 4478–4482. https://doi.org/10.4049/jimmunol.1203172.
43. Lee, P.P., Fitzpatrick, D.R., Beard, C., Jessup, H.K., Lehar, S., Makar, K.W., Pérez-Melgosa, M., Sweetser, M.T., Schlissel, M.S., Nguyen, S., et al. (2001). A Critical Role for Dnmt1 and DNA Methylation in T Cell Development, Function, and Survival. Immunity *15*, 763–774. https://doi.org/10.1016/S1074-7613(01)00227-8.
44. Khader, S.A., Gaffen, S.L., and Kolls, J.K. (2009). Th17 cells at the crossroads of innate and adaptive immunity against infectious diseases at the mucosa. Mucosal Immunol. *2*, 403–411. https://doi.org/10.1038/mi.2009.100.
45. Laurence, A., Tato, C.M., Davidson, T.S., Kanno, Y., Chen, Z., Yao, Z., Blank, R.B., Meylan, F., Siegel, R., Hennighausen, L., et al. (2007). Interleukin-2 Signaling via STAT5 Constrains T Helper 17 Cell Generation. Immunity *26*, 371–381. https://doi.org/10.1016/j.immuni.2007.02.009.
46. Liao, W., Lin, J.-X., and Leonard, W.J. (2013). Interleukin-2 at the Crossroads of Effector Responses, Tolerance, and Immunotherapy. Immunity *38*, 13–25. https://doi.org/10.1016/j.immuni.2013.01.004.
47. Kim, H.S., Jang, S.W., Lee, W., Kim, K., Sohn, H., Hwang, S.S., and Lee, G.R. (2017). PTEN drives Th17 cell differentiation by preventing IL-2 production. J. Exp. Med. *214*, 3381–3398. https://doi.org/10.1084/jem.20170523.
48. Panagoulias, I., Georgakopoulos, T., Aggeletopoulou, I., Agelopoulos, M., Thanos, D., and Mouzaki, A. (2016). Transcription Factor Ets-2 Acts as a Preinduction Repressor of Interleukin-2 (IL-2) Transcription in Naive T Helper Lymphocytes. J. Biol. Chem. *291*, 26707–26721. https://doi.org/10.1074/jbc.M116.762179.
49. Liao, W., Lin, J.-X., Wang, L., Li, P., and Leonard, W.J. (2011). Modulation of cytokine receptors by IL-2 broadly regulates differentiation into helper T cell lineages. Nat. Immunol. *12*, 551–559. https://doi.org/10.1038/ni.2030.
50. Yang, X.-P., Ghoreschi, K., Steward-Tharp, S.M., Rodriguez-Canales, J., Zhu, J., Grainger, J.R., Hirahara, K., Sun, H.-W., Wei, L., Vahedi, G., et al. (2011). Opposing regulation of the locus encoding IL-17 through direct, reciprocal actions of STAT3 and STAT5. Nat. Immunol. *12*, 247–254. https://doi.org/10.1038/ni.1995.
51. Evans, C.M., and Jenner, R.G. (2013). Transcription factor interplay in t helper cell differentiation. Brief. Funct. Genomics *12*, 499–511. https://doi.org/10.1093/bfgp/elt025.
52. Avni, O., and Rao, A. (2000). T cell differentiation: a mechanistic view. Curr. Opin. Immunol. *12*, 654–659. https://doi.org/10.1016/S0952-7915(00)00158-8.

53. Murphy, K.M., and Reiner, S.L. (2002). The lineage decisions of helper T cells. Nat. Rev. Immunol. *2*, 933–944. https://doi.org/10.1038/nri954.

54. Harris, T.J., Grosso, J.F., Yen, H.-R., Xin, H., Kortylewski, M., Albesiano, E., Hipkiss, E.L., Getnet, D., Goldberg, M.V., Maris, C.H., et al. (2007). Cutting Edge: An In Vivo Requirement for STAT3 Signaling in TH17 Development and TH17-Dependent Autoimmunity. J. Immunol. *179*, 4313–4317. https://doi.org/10.4049/jimmunol.179.7.4313.

55. Ivanov, I.I., McKenzie, B.S., Zhou, L., Tadokoro, C.E., Lepelley, A., Lafaille, J.J., Cua, D.J., and Littman, D.R. (2006). The Orphan Nuclear Receptor RORγt Directs the Differentiation Program of Proinflammatory IL-17+ T Helper Cells. Cell *126*, 1121–1133. https://doi.org/10.1016/j.cell.2006.07.035.

56. Korn, T., Bettelli, E., Gao, W., Awasthi, A., Jäger, A., Strom, T.B., Oukka, M., and Kuchroo, V.K. (2007). IL-21 initiates an alternative pathway to induce proinflammatory TH17 cells. Nature *448*, 484–487. https://doi.org/10.1038/nature05970.

57. Schraml, B.U., Hildner, K., Ise, W., Lee, W.-L., Smith, W.A.E., Solomon, B., Sahota, G., Sim, J., Mukasa, R., Cemerski, S., et al. (2009). The AP-1 transcription factor Batf controls TH17 differentiation. Nature *460*, 405–409. https://doi.org/10.1038/nature08114.

58. Awasthi, A., Riol-Blanco, L., Jäger, A., Korn, T., Pot, C., Galileos, G., Bettelli, E., Kuchroo, V.K., and Oukka, M. (2009). Cutting Edge: IL-23 Receptor GFP Reporter Mice Reveal Distinct Populations of IL-17-Producing Cells. J. Immunol. *182*, 5904–5908. https://doi.org/10.4049/jimmunol.0900732.

59. Nath, N., Prasad, R., Giri, S., Singh, A.K., and Singh, I. (2006). T-bet is essential for the progression of experimental autoimmune encephalomyelitis. Immunology (Oxf.) *118*, 384–391. https://doi.org/10.1111/j.1365-2567.2006.02385.x.

60. Yang, Y., Weiner, J., Liu, Y., Smith, A.J., Huss, D.J., Winger, R., Peng, H., Cravens, P.D., Racke, M.K., and Lovett-Racke, A.E. (2009). T-bet is essential for encephalitogenicity of both Th1 and Th17 cells. J. Exp. Med. *206*, 1549–1564. https://doi.org/10.1084/jem.20082584.

61. International Multiple Sclerosis Genetics Consortium IMSGC, Beecham, A.H., Patsopoulos, N.A., Xifara, D.K., Davis, M.F., Kemppinen, A., Cotsapas, C., Shah, T.S., Spencer, C., Booth, D., et al. (2013). Analysis of immune-related loci identifies 48 new susceptibility variants for multiple sclerosis. Nat. Genet. *45*, 1353–1360. https://doi.org/10.1038/ng.2770.

62. Sun, J., Yi, S., Qiu, L., Fu, W., Wang, A., Liu, F., Wang, L., Wang, T., Chen, H., Wang, L., et al. (2018). SATB1 Defines a Subtype of Cutaneous CD30 + Lymphoproliferative Disorders Associated with a T-Helper 17 Cytokine Profile. J. Invest. Dermatol. *138*, 1795–1804. https://doi.org/10.1016/j.jid.2018.02.028.

63. Kumar, P.P., Purbey, P.K., Ravi, D.S., Mitra, D., and Galande, S. (2005). Displacement of SATB1-Bound Histone Deacetylase 1 Corepressor by the Human Immunodeficiency Virus Type 1 Transactivator Induces Expression of Interleukin-2 and Its Receptor in T Cells. Mol. Cell Biol. *25*, 1620–1633. https://doi.org/10.1128/MCB.25.5.1620-1633.2005.

64. Pavan Kumar, P., Purbey, P.K., Sinha, C.K., Notani, D., Limaye, A., Jayani, R.S., and Galande, S. (2006). Phosphorylation of SATB1, a Global Gene Regulator, Acts as a Molecular Switch Regulating Its Transcriptional Activity In Vivo. Mol. Cell *22*, 231–243. https://doi.org/10.1016/j.molcel.2006.03.010.

65. Boyman, O., and Sprent, J. (2012). The role of interleukin-2 during homeostasis and activation of the immune system. Nat. Rev. Immunol. *12*, 180–190. https://doi.org/10.1038/nri3156.

66. Peters, A., Fowler, K.D., Chalmin, F., Merkler, D., Kuchroo, V.K., and Pot, C. (2015). IL-27 Induces Th17 Differentiation in the Absence of STAT1 Signaling. J. Immunol. *195*, 4144–4153. https://doi.org/10.4049/jimmunol.1302246.

67. Durant, L., Watford, W.T., Ramos, H.L., Laurence, A., Vahedi, G., Wei, L., Takahashi, H., Sun, H.-W., Kanno, Y., Powrie, F., and O'Shea, J.J. (2010). Diverse Targets of the Transcription Factor STAT3 Contribute to T Cell Pathogenicity and Homeostasis. Immunity *32*, 605–615. https://doi.org/10.1016/j.immuni.2010.05.003.

68. Ghoreschi, K., Laurence, A., Yang, X.P., Tato, C.M., McGeachy, M.J., Konkel, J.E., Ramos, H.L., Wei, L., Davidson, T.S., Bouladoux, N., et al. (2010). Generation of pathogenic T(H)17 cells in the absence of TGF-β signalling. Nature *467*, 967–971. https://doi.org/10.1038/nature09447.

69. Qin, Z., Wang, R., Hou, P., Zhang, Y., Yuan, Q., Wang, Y., Yang, Y., and Xu, T. (2024). TCR signaling induces STAT3 phosphorylation to promote TH17 cell differentiation. J. Exp. Med. *221*, e20230683. https://doi.org/10.1084/jem.20230683.

70. Purwar, R., Schlapbach, C., Xiao, S., Kang, H.S., Elyaman, W., Jiang, X., Jetten, A.M., Khoury, S.J., Fuhlbrigge, R.C., Kuchroo, V.K., et al. (2012). Robust tumor immunity to melanoma mediated by interleukin-9-producing T cells. Nat. Med. *18*, 1248–1253. https://doi.org/10.1038/nm.2856.

71. Huang, W., Thomas, B., Flynn, R.A., Gavzy, S.J., Wu, L., Kim, S.V., Hall, J.A., Miraldi, E.R., Ng, C.P., Rigo, F., et al. (2015). DDX5 and its associated lncRNA Rmrp modulate TH17 cell effector functions. Nature *528*, 517–522. https://doi.org/10.1038/nature16193.

72. Chi, X., Jin, W., Zhao, X., Xie, T., Shao, J., Bai, X., Jiang, Y., Wang, X., and Dong, C. (2022). RORγt expression in mature T_H17 cells safeguards their lineage specification by inhibiting conversion to T_H2 cells. Sci. Adv. *8*, eabn7774. https://doi.org/10.1126/sciadv.abn7774.

73. Zhong, X., Wu, H., Zhang, W., Gwack, Y., Shang, W., Lee, K.O., Isakov, N., He, Z., and Sun, Z. (2022). Decoupling the role of RORγt in the differentiation and effector function of T_H17 cells. Sci. Adv. *8*, eadc9221. https://doi.org/10.1126/sciadv.adc9221.

74. Shinkai, Y., Rathbun, G., Lam, K.-P., Oltz, E.M., Stewart, V., Mendelsohn, M., Charron, J., Datta, M., Young, F., Stall, A.M., and Alt, F.W. (1992). RAG-2-deficient mice lack mature lymphocytes owing to inability to initiate V(D)J rearrangement. Cell *68*, 855–867. https://doi.org/10.1016/0092-8674(92)90029-C.

75. Sasaki, Y., Derudder, E., Hobeika, E., Pelanda, R., Reth, M., Rajewsky, K., and Schmidt-Supprian, M. (2006). Canonical NF-κB Activity, Dispensable for B Cell Development, Replaces BAFF-Receptor Signals and Promotes B Cell Proliferation upon Activation. Immunity *24*, 729–739. https://doi.org/10.1016/j.immuni.2006.04.005.

76. Langmead, B., and Salzberg, S.L. (2012). Fast gapped-read alignment with Bowtie 2. Nat. Methods *9*, 357–359. https://doi.org/10.1038/nmeth.1923.

77. Ramírez, F., Ryan, D.P., Grüning, B., Bhardwaj, V., Kilpert, F., Richter, A.S., Heyne, S., Dündar, F., and Manke, T. (2016). deepTools2: a next generation web server for deep-sequencing data analysis. Nucleic Acids Res. *44*, W160–W165. https://doi.org/10.1093/nar/gkw257.

78. Zhang, Y., Liu, T., Meyer, C.A., Eeckhoute, J., Johnson, D.S., Bernstein, B.E., Nusbaum, C., Myers, R.M., Brown, M., Li, W., and Liu, X.S. (2008). Model-based Analysis of ChIP-Seq (MACS). Genome Biol. *9*, R137. https://doi.org/10.1186/gb-2008-9-9-r137.

79. Li, H., Handsaker, B., Wysoker, A., Fennell, T., Ruan, J., Homer, N., Marth, G., Abecasis, G., and Durbin, R.; 1000 Genome Project Data Processing Subgroup (2009). The Sequence Alignment/Map format and SAMtools. Bioinformatics *25*, 2078–2079. https://doi.org/10.1093/bioinformatics/btp352.

80. Dobin, A., Davis, C.A., Schlesinger, F., Drenkow, J., Zaleski, C., Jha, S., Batut, P., Chaisson, M., and Gingeras, T.R. (2013). STAR: ultrafast universal RNA-seq aligner. Bioinformatics *29*, 15–21. https://doi.org/10.1093/bioinformatics/bts635.

81. Bolger, A.M., Lohse, M., and Usadel, B. (2014). Trimmomatic: a flexible trimmer for Illumina sequence data. Bioinformatics *30*, 2114–2120. https://doi.org/10.1093/bioinformatics/btu170.

82. Butler, A., Hoffman, P., Smibert, P., Papalexi, E., and Satija, R. (2018). Integrating single-cell transcriptomic data across different conditions, technologies, and species. Nat. Biotechnol. *36*, 411–420. https://doi.org/10.1038/nbt.4096.

83. Stuart, T., Srivastava, A., Madad, S., Lareau, C.A., and Satija, R. (2021). Single-cell chromatin state analysis with Signac. Nat. Methods *18*, 1333–1341. https://doi.org/10.1038/s41592-021-01282-5.

84. Yu, G., Wang, L.-G., Han, Y., and He, Q.-Y. (2012). clusterProfiler: an R Package for Comparing Biological Themes Among Gene Clusters. OMICS A J. Integr. Biol. *16*, 284–287. https://doi.org/10.1089/omi.2011.0118.

85. Sayols, S. (2023). rrvgo: a Bioconductor package for interpreting lists of Gene Ontology terms. MicroPubl. Biol. *2023*. https://doi.org/10.17912/micropub.biology.000811.

86. Pliner, H.A., Packer, J.S., McFaline-Figueroa, J.L., Cusanovich, D.A., Daza, R.M., Aghamirzaie, D., Srivatsan, S., Qiu, X., Jackson, D., Minkina, A., et al. (2018). Cicero Predicts cis-Regulatory DNA Interactions from Single-Cell Chromatin Accessibility Data. Mol. Cell *71*, 858–871.e8. https://doi.org/10.1016/j.molcel.2018.06.044.

87. Fornes, O., Castro-Mondragon, J.A., Khan, A., van der Lee, R., Zhang, X., Richmond, P.A., Modi, B.P., Correard, S., Gheorghe, M., Baranašić, D., et al. (2020). JASPAR 2020: update of the open-access database of transcription factor binding profiles. Nucleic Acids Res. *48*, D87–D92. https://doi.org/10.1093/nar/gkz1001.

88. Lawrence, M., Huber, W., Pagès, H., Aboyoun, P., Carlson, M., Gentleman, R., Morgan, M.T., and Carey, V.J. (2013). Software for Computing and Annotating Genomic Ranges. PLoS Comput. Biol. *9*, e1003118. https://doi.org/10.1371/journal.pcbi.1003118.

89. Tan, G., and Lenhard, B. (2016). TFBSTools: an R/bioconductor package for transcription factor binding site analysis. Bioinformatics *32*, 1555–1556. https://doi.org/10.1093/bioinformatics/btw024.

90. Bebo, B.F., Dehghani, B., Foster, S., Kurniawan, A., Lopez, F.J., and Sherman, L.S. (2009). Treatment with selective estrogen receptor modulators regulates myelin specific T-cells and suppresses experimental autoimmune encephalomyelitis. GLIA (New York, N. Y.) *57*, 777–790. https://doi.org/10.1002/glia.20805.

91. Poppensieker, K., Otte, D.M., Schürmann, B., Limmer, A., Dresing, P., Drews, E., Schumak, B., Klotz, L., Raasch, J., Mildner, A., et al. (2012). CC chemokine receptor 4 is required for experimental autoimmune encephalomyelitis by regulating GM-CSF and IL-23 production in dendritic cells. Proc. Natl. Acad. Sci. USA *109*, 3897–3902. https://doi.org/10.1073/pnas.1114153109.

92. Brandstätter, O., Schanz, O., Vorac, J., König, J., Mori, T., Maruyama, T., Korkowski, M., Haarmann-Stemmann, T., von Smolinski, D., Schultze, J. L., et al. (2016). Balancing intestinal and systemic inflammation through cell type-specific expression of the aryl hydrocarbon receptor repressor. Sci. Rep. *6*, 26091. https://doi.org/10.1038/srep26091.

93. Fujimura, K., Oyamada, A., Iwamoto, Y., Yoshikai, Y., and Yamada, H. (2013). CD4 T cell-intrinsic IL-2 signaling differentially affects Th1 and Th17 development. J. Leukoc. Biol. *94*, 271–279. https://doi.org/10.1189/jlb.1112581.

94. Bonaguro, L., Köhne, M., Schmidleithner, L., Schulte-Schrepping, J., Warnat-Herresthal, S., Horne, A., Kern, P., Günther, P., ter Horst, R., Jaeger, M., et al. (2020). CRELD1 modulates homeostasis of the immune system in mice and humans. Nat. Immunol. *21*, 1517–1527. https://doi.org/10.1038/s41590-020-00811-2.

95. Schmidleithner, L., Thabet, Y., Schönfeld, E., Köhne, M., Sommer, D., Abdullah, Z., Sadlon, T., Osei-Sarpong, C., Subbaramaiah, K., Copperi, F., et al. (2019). Enzymatic Activity of HPGD in Treg Cells Suppresses Tconv Cells to Maintain Adipose Tissue Homeostasis and Prevent Metabolic Dysfunction. Immunity *50*, 1232–1248.e1214. https://doi.org/10.1016/j.immuni.2019.03.014.

96. ten Hove, T., van den Blink, B., Pronk, I., Drillenburg, P., Peppelenbosch, M.P., and van Deventer, S.J.H. (2002). Dichotomal role of inhibition of p38 MAPK with SB 203580 in experimental colitis. Gut *50*, 507–512. https://doi.org/10.1136/gut.50.4.507.

97. Ellwardt, E., Pramanik, G., Luchtman, D., Novkovic, T., Jubal, E.R., Vogt, J., Arnoux, I., Vogelaar, C.F., Mandal, S., Schmalz, M., et al. (2018). Maladaptive cortical hyperactivity upon recovery from experimental autoimmune encephalomyelitis. Nat. Neurosci. *21*, 1392–1403. https://doi.org/10.1038/s41593-018-0193-2.

98. Love, M.I., Huber, W., and Anders, S. (2014). Moderated estimation of fold change and dispersion for RNA-seq data with DESeq2. Genome Biol. *15*, 550. https://doi.org/10.1186/s13059-014-0550-8.

99. Ignatiadis, N., Klaus, B., Zaugg, J.B., and Huber, W. (2016). Data-driven hypothesis weighting increases detection power in genome-scale multiple testing. Nat. Methods *13*, 577–580. https://doi.org/10.1038/nmeth.3885.

100. Liberzon, A., Birger, C., Thorvaldsdóttir, H., Ghandi, M., Mesirov, J.P., and Tamayo, P. (2015). The Molecular Signatures Database (MSigDB) hallmark gene set collection. Cell Syst. *1*, 417–425. https://doi.org/10.1016/j.cels.2015.12.004.

101. Hao, Y., Hao, S., Andersen-Nissen, E., Mauck, W.M., 3rd, Zheng, S., Butler, A., Lee, M.J., Wilk, A.J., Darby, C., Zager, M., et al. (2021). Integrated analysis of multimodal single-cell data. Cell *184*, 3573–3587.e29. https://doi.org/10.1016/j.cell.2021.04.048.

102. Korsunsky, I., Millard, N., Fan, J., Slowikowski, K., Zhang, F., Wei, K., Baglaenko, Y., Brenner, M., Loh, P.R., and Raychaudhuri, S. (2019). Fast, sensitive and accurate integration of single-cell data with Harmony. Nat. Methods *16*, 1289–1296. https://doi.org/10.1038/s41592-019-0619-0.

103. Buenrostro, J.D., Giresi, P.G., Zaba, L.C., Chang, H.Y., and Greenleaf, W. J. (2013). Transposition of native chromatin for fast and sensitive epigenomic profiling of open chromatin, DNA-binding proteins and nucleosome position. Nat. Methods *10*, 1213–1218. https://doi.org/10.1038/nmeth.2688.

104. Picelli, S., Björklund, A.K., Reinius, B., Sagasser, S., Winberg, G., and Sandberg, R. (2014). Tn5 transposase and tagmentation procedures for massively scaled sequencing projects. Genome Res. *24*, 2033–2040. https://doi.org/10.1101/gr.177881.114.

105. Yu, G., Wang, L.-G., and He, Q.-Y. (2015). ChIPseeker: an R/Bioconductor package for ChIP peak annotation, comparison and visualization. Bioinformatics *31*, 2382–2383. https://doi.org/10.1093/bioinformatics/btv145.

106. Ashburner, M., Ball, C.A., Blake, J.A., Botstein, D., Butler, H., Cherry, J. M., Davis, A.P., Dolinski, K., Dwight, S.S., Eppig, J.T., et al. (2000). Gene Ontology: tool for the unification of biology. Nat. Genet. *25*, 25–29. https://doi.org/10.1038/75556.

107. Carbon, S., Douglass, E., Dunn, N., Good, B., Harris, N.L., Lewis, S.E., Mungall, C.J., Basu, S., Chisholm, R.L., Dodson, R.J., et al. (2019). The Gene Ontology Resource: 20 years and still GOing strong. Nucleic Acids Res. *47*, D330–D338. https://doi.org/10.1093/nar/gky1055.

108. Wang, Y.S., Chiu, W.T., Chang, F.P., and Chen, Y.L. (1988). Decline of chlorinated hydrocarbon insecticides residues in the tea-garden soils of Taiwan. Proc. Natl. Sci. Counc. Repub. China B *12*, 9–13.

109. The Gene Ontology Consortium (2019). The Gene Ontology Resource: 20 years and still GOing strong. Nucleic Acids Res. *47*, D330–D338. https://doi.org/10.1093/nar/gky1055.

110. Wu, T., Hu, E., Xu, S., Chen, M., Guo, P., Dai, Z., Feng, T., Zhou, L., Tang, W., Zhan, L., et al. (2021). clusterProfiler 4.0: A universal enrichment tool for interpreting omics data. Innovation *2*, 100141. https://doi.org/10.1016/j.xinn.2021.100141.

STAR★METHODS

KEY RESOURCES TABLE

REAGENT or RESOURCE	SOURCE	IDENTIFIER
Antibodies		
Anti-Actin Antibody, Clone: C4	Millipore	Cat# MAB1501; RRID:AB_2223041
Anti-Bcl-2 PE-Cy7, Clone: BCL/10C4	BioLegend	Cat# 633511; RRID:AB_2565246
Anti-BrdU BV510, Clone: 3D4	BioLegend	Cat# 364119; RRID:AB_3105984
Anti-Caspase3 PE, Clone: C92-605.rMAb	BD Biosciences	Cat# 570183
Anti-CD107b (MAC3), Clone: M8/84	BD Bioscience	Cat# 553322; RRID:AB_394780
Anti-CD11b BV605, Clone: M1/70	Biolegend	Cat# 101237; RRID:AB_11126744
Anti-CD126 (IL6R) PE-Cy7, Clone: D7715A7	Thermo Fisher Scientific	Cat# 25-1261-80; RRID:AB_2573391
Anti-CD25 Alexa Fluor 647, Clone: PC61	Biolegend	Cat# 102020; RRID:AB_493458
Anti-CD25 APC-Cy7, Clone: PC61	Biolegend	Cat# 102026; RRID:AB_830745
Anti-CD25 BV510, Clone: PC61	Biolegend	Cat# 102042; RRID:AB_2562270
Anti-CD25 BV650, Clone: PC61	BD Biosciences	Cat# 564021; RRID:AB_2738547
Anti-CD25 PE-Cy7, Clone: PC61	Biolegend	Cat# 102016; RRID:AB_312865
Anti-CD3, Clone: CD3-12	Bio-Rad	Cat# MCA1477T; RRID:AB_10845948
Anti-CD3 APC, Clone: 17A2	Thermo Fisher Scientific	Cat# 17-0032-82; RRID:AB_10597589
Anti-CD3 BUV737, Clone: 145-2C11	BD Biosciences	Cat# 564618; RRID:AB_2738868
Anti-CD3 BV510, Clone: 17A2	Biolegend	Cat# 100234; RRID:AB_2562555
Anti-CD3 BV650, Clone: 17A2	Biolegend	Cat# 100229; RRID:AB_11204249
Anti-CD3 FITC, Clone: 17A2	Biolegend	Cat# 100203; RRID:AB_312660
Anti-CD3 PE-eFluor 610, Clone: 145-2C11	Thermo Fisher Scientific	Cat# 61-0031-80; RRID:AB_2574513
Anti-CD304 (Neuropilin) PE-Cy7, Clone 3E12	BioLegend	Cat# 145212; RRID:AB_2562360
Anti-CD357 (GITR) BUV615, Clone: DTA-1	BD Biosciences	Cat# 751532; RRID:AB_2875527
Anti-CD4 APC-Cy7, Clone: RM4-5	Biolegend	Cat# 100526; RRID:AB_312727
Anti-CD4 BV510, Clone: RM4-5	Biolegend	Cat# 100553; RRID:AB_2561388
Anti-CD4 BV650, Clone: RM4-5	Biolegend	Cat# 100555; RRID:AB_2562529
Anti-CD4 BV785, Clone: RM4-5	Biolegend	Cat# 100552; RRID:AB_2563053
Anti-CD4 BUV395, Clone: RM4-5	BD Biosciences	Cat# 568375; RRID:AB_3095981
Anti-CD4 PerCP/Cyanine5.5, Clone: RM4-5	Biolegend	Cat# 100540; RRID:AB_893326
Anti-CD44 BV605, Clone: IM7	Biolegend	Cat# 103047; RRID:AB_2562451
Anti-CD44 Pacific Blue, Clone: IM7	Biolegend	Cat# 103020; RRID:AB_493683
Anti-CD45 BV570, Clone: 30-F11	Biolegend	Cat# 103135; RRID:AB_10898325
Anti-CD45 AF488, Clone: 30-F11	Biolegend	Cat# 103122; RRID:AB_493531
Anti-CD62L APC-eFluor 780, Clone: MEL-14	Thermo Fisher Scientific	Cat# 47-0621-80; RRID:AB_1603258
Anti-CD62L BV786, Clone: MEL-14	BD Biosciences	Cat# 564109; RRID:AB_2738598
Anti-CD62L PE-Cy7, Clone: MEL-14	Biolegend	Cat# 104418; RRID:AB_313103
Anti-CTLA-4 APC, Clone: UC10-4F10-11	BD Biosciences	Cat# 564331; RRID:AB_2738751
Anti-FoxP3 efluor 450, Clone: FJK-16s	Thermo Fisher Scientific	Cat# 48-5773-82; RRID:AB_1518812
Anti-FoxP3 PE, Clone: MF-14	Biolegend	Cat# 126404; RRID:AB_1089117
Anti-Foxp3 PE-eFluor 610, Clone: FJK-16s	eBioscience	Cat# 61-5773-80; RRID:AB_2574623
Anti-GATA3 PE-CF594, Clone: L50-823	BD	Cat# 563510; RRID:AB_2738248
Anti-GM-CSF PE-Cy7, Clone: MP1-22E9	BioLegend	Cat# 505411; RRID:AB_2721681
Anti-GM-CSF PerCP/Cyanine5.5, Clone: MP1-22E9	Biolegend	Cat# 505410; RRID:AB_2562376
Anti-IFNγ PE-Cy7, Clone: XMG1.2	Thermo Fisher Scientific	Cat# 25-7311-82; RRID:AB_469680
Anti-IFNγ BUV805, Clone: XMG1.2	BD Biosciences	Cat# 569625

(*Continued on next page*)

Continued

REAGENT or RESOURCE	SOURCE	IDENTIFIER
Anti-IL-10 APC, Clone: JES5-16E3	Biolegend	Cat# 505010; RRID:AB_315364
Anti-IL-17 PE, Clone: eBio17B7	Thermo Fisher Scientific	Cat# 12-7177-81; RRID:AB_763582
Anti-IL-2 eFluor 450, Clone: JES6-5H4	Thermo Fisher Scientific	Cat# 48-7021-82; RRID:AB_1944462
Anti-IL-4 APC, Clone: 11B11	Thermo Fisher Scientific	Cat# 17-7041-82; RRID:AB_469494
Anti-IL-4 PE/Dazzle^{TM} 594, Clone: 11B11	Biolegend	Cat# 504132; RRID:AB_2564559
Anti- Ki-67 BV786, Clone: B56	BD Biosciences	Cat# 563756; RRID:AB_2732007
Anti-Ki-67 Pe-eFluor 610, Clone: SolA15	Thermo Fisher Scientific	Cat# 61-5698-82; RRID:AB_2574620
Anti-Ly6G APC, Clone: 1A8-Ly6g	Thermo Fisher Scientific	Cat# 17-9668-82; RRID:AB_2573307
Anti-mouse IgG Antibody, HRP conjugated	GE Healthcare	Cat# NA9340-1ml; RRID:AB_772191
Anti-Phospho-STAT3 (Tyr705) eFluor 450, Clone: LUVNKLA	Thermo Fisher Scientific	Cat# 48-9033-42; RRID:AB_2574121
Anti-Phospho-STAT5 (Tyr694) PE, Clone: SRBCZX	Thermo Fisher Scientific	Cat# 12-9010-42; RRID:AB_2572671
Anti-rabbit IgG Antibody, HRP conjugated	GE Healthcare	Cat# GENA934; RRID:AB_2722659
Anti-RORγt APC, Clone: AFKJS-9	Thermo Fisher Scientific	Cat# 17-6988-82; RRID:AB_10609207
Anti-RORγt PE, Clone: B2D	Thermo Fisher Scientific	Cat# 12-6981-82; RRID:AB_10807092
Anti-Satb1, Clone: EPR3951	Abcam	Cat# ab109122; RRID:AB_10862207
Anti-Satb1 Alexa Fluor 647, Clone: 14/SATB1	BD Biosciences	Cat# 562378; RRID:AB_11153310
Anti-Tbet efluor 660, Clone: eBio4B10	Thermo Fisher Scientific	Cat# 50-5825-82; RRID:AB_10596655
Anti-TNF-α BV510, Clone: MP6-XT22	Biolegend	Cat# 506339; RRID:AB_2563127
goat affinity purified antibody to hamster IgG (whole molecule)	MP Biomedicals	Cat# 0856984; RRID:AB_2334783
LEAF Purified anti-CD28, Clone: 37.51	Biolegend	Cat# 102112; RRID:AB_312877
LEAF Purified anti-CD3, Clone: 145-2C11	Biolegend	Cat# 100314; RRID:AB_312679
LEAF Purified anti-IFNγ, Clone: R4-6A2	Biolegend	Cat# 505706; RRID:AB_315394
LEAF Purified anti-IL-4, Clone: 11B11	Biolegend	Cat# 504108; RRID:AB_315322
LEAF Purified anti-mouse CD25 antibody, Clone: PC61	Biolegend	Cat# 102014; RRID:AB_312863
LEAF Purified anti-mouse IL-2 antibody, Clone: JES6-1A12	Biolegend	Cat# 503704; RRID:AB_315294
Purified anti-mouse CD16/32 antibody, Clone: 93	Biolegend	Cat# 101302; RRID:AB_312801
Bacterial and virus strains		
E.coli K12, strain DH5α	DSMZ	DSM# 6897
E.coli, strain Stbl3	Thermo Fisher Scientific	Cat# C737303
Chemicals, peptides, and recombinant proteins		
2-Desoxy-D-Glucose (2DG)	Carl Roth	Cat# CN96.2
4-OH Tamoxifen	Merck	Cat# H7904
Adjuvant, Complete H37 Ra	BD	Cat# 231131
AgeI-HF	NEB	Cat# R3552S
Antimycin A	Merck	Cat# A8674
Collagenase, type IV	Merck	Cat# C5138
cOmplete Protease Inhibitor Cocktail	Roche	Cat# 04693116001
CountBright absolute counting beads	Thermo Fisher Scientific	Cat# C36950
DNAse I, from bovine pancreas	Merck	Cat# 11284932001
DNAse I, grade II, from bovine pancreas	Merck	Cat# 10104159001
Dynabeads Mouse T-Activator CD3/CD28 for T Cell Expansion and Activation	Thermo Fisher Scientific	Cat# 11456D
eBioscience Cell Proliferation Dye eFluor 670	Thermo Fisher Scientific	Cat# 65-0840-85
eBioscience Cell stimulation cocktail	Thermo Fisher Scientific	Cat# 00-4970-03
eBioscience Brefeldin A Solution (1000x)	Thermo Fisher Scientific	Cat# 00-4506-51

(*Continued on next page*)

Continued

REAGENT or RESOURCE	SOURCE	IDENTIFIER
eBioscience Monensin Solution (1000x)	Thermo Fisher Scientific	Cat# 00-4505-51
eBioscience Permeabilization Buffer (10X)	Thermo Fisher Scientific	Cat# 00-8333-56
ECL Western blot substrate	Merck	Cat# GERPN2106
EcoRI-HF	NEB	Cat# R3101
FCCP	Merck	Cat# C2920
Gibco DMEM medium	Thermo Fisher Scientific	Cat# 41965039
Gibco IMDM medium	Thermo Fisher Scientific	Cat# 12440053
High Sensitivity D1000 Reagents	Agilent	Cat# 5067-5585
High Sensitivity D1000 ScreenTape	Agilent	Cat# 5067-5584
IGEPAL CA-630	Merck	Cat# I8896
IL-2 (Proleukin)	Chiron/Novartis	PZN# 2238131
KpnI-HF	NEB	Cat# R3142
Liberase	Merck	Cat# 05401127001
LightCycler 480 Probes Master	Roche	Cat# 4887301001
Ms nucleoporin p62 Sample Tag 5-9	BD Biosciences	Cat# 460293-460296
Mycobacterium tuberculosis H37Ra, desiccated	BD	Cat# 231141
Myelin oligodendrocyte glycoprotein (MOG) 35-55 peptide	Biotrend	Cat# BP0328
NEBNext High-Fidelity 2X PCR Master Mix	NEB	Cat# M0541
Nuclear Fast Red solution	Merck	Cat# N3020
NuPAGE LDS Sample Buffer	Thermo Fisher Scientific	Cat# NP0007
NuPAGE Sample Reducing Agent	Thermo Fisher Scientific	Cat# NP0009
Oligomycin A	Merck	Cat# 75351
Pertussis Toxin	Merck	Cat# P2980
Pierce 16% Formaldehyde (w/v), Methanol	Thermo Fisher Scientific	Cat# 28908
poly-L-lysine	Merck	Cat# P5899
QIAzol Lysis Reagent	Qiagen	Cat# 79306
RNase Inhibitor	BD Biosciences	Cat# 51-9024039
Recombinant human TGF-β1 (HEK293 derived)	PeproTech	Cat# 100-21
Retinoic acid	Merck	Cat# R2625
rm IL-12	PeproTech	Cat# 210-12
rm IL-4	Immunotools	Cat# 12340045
rm IL-6	Immunotools	Cat# 12340065
Rotenone	Merck	Cat# R8875
Seahorse XF RPMI Medium pH 7.4	Agilent	Cat# 103576-100
SeeBlue Plus2 Pre-stained Protein Standard	Thermo Scientific	Cat# LC5925
Solvent blue 38	Merck	Cat# S3382
Tamoxifen	Merck	Cat# T5648
TAPS	Merck	Cat# T5130
TN5 Tansposase	Matthias Geyer	N/D
Critical commercial assays		
Agilent Seahorse XF96 Cell Culture Microplates	Agilent	Cat# 101085-004
BD Rhapsody 8-Lane Cartridge	BD Biosciences	Cat# 666262
BD Rhapsody cDNA Kit	BD Biosciences	Cat# 633773
BD Rhapsody Enhanced Cartridge Reagent Kit V3a	BD Biosciences	Cat# 667052
BD Rhapsody Immune Response Panel Mm	BD Biosciences	Cat# 633753
BD Rhapsody Multiomic ATAC-Seq Amplification Kit	BD Biosciences	Cat 41928
BD Rhapsody Tagmentation and Supplemental Reagents Kit	BD Biosciences	Cat# 41926
BD Rhapsody WTA Amplification Kit	BD Biosciences	Cat# 633801

(*Continued on next page*)

Continued

REAGENT or RESOURCE	SOURCE	IDENTIFIER
Direct-zol-96 RNA Kit	Zymo Research	Cat# R2054
ebioscience Foxp3 / Transcription Factor Staining Buffer Set	Thermo Fisher Scientific	Cat# 00-5523-00
LEGENDplex MU Th Cytokine Panel (12-plex) w/ FP V03	Biolegend	Cat# 741043
LIVE/DEAD Fixable Near-IR Dead Cell Stain Kit	Thermo Fisher Scientific	Cat# L10119
LIVE/DEAD Fixable Yellow Dead Cell Stain Kit	Thermo Fisher Scientific	Cat# L34959
MagniSort Mouse CD4 T cell Enrichment Kit	Thermo Fisher Scientific	Cat# 8804-6821-74
MinElute PCR Purification Kit	Qiagen	Cat# 28006
miRNeasy Micro Kit	Qiagen	Cat# 217084
Pkh26 Red Fluorescent Cell Linker Kit	Sigma-Aldrich	Cat# PKH26GL-1KT
Phase-Flow BrdU cell proliferation kit for flow cytometry	Biolegend	Cat# 370706
Transcriptor First Strand cDNA synthesis kit	Roche	Cat# 4897030001
TruSeq SR Cluster kit v3	Illumina	Cat# GD-401-3001
TruSeq SBS Kit v3 (50 cycles)	Illumina	Cat# FC-401-3002
TruSeq RNA Library Prep Kit v2	Illumina	Cat# RS-122-2001
Universal ProbeLibrary Set, Human	Roche	Cat# 4683633001
Deposited data		
ATAC-seq Data	This paper	GSE250576
Bulk RNA-seq Data	This paper	GSE250577
scRNA-seq Data	This paper	GSE250578
scMultiOMICs Data	This paper	GSE290258
ChIP-seq data (H3K4me2, H3K4me3, Stat3, RORγt)	Ciofani et al.[33]	GSE40918
ChIP-seq data (H3Ac, Stat3)	Ghoreschi et al.[68]	GSE23681
Affymetrix Expression Data	Durant et al.[67]	GSE21670
RNA-seq Data	Ciofani et al.[33]	GSE40918
RNA-seq Data	Qin et al.[69]	GSE229377
Agilent Expression Data	Purwar et al.[70]	GSE38704
RNA-seq Data	Huang et al.[71]	GSE70108
RNA-seq Data	Chi et al.[72]	GSE190538
RNA-seq Data	Zhong et al.[73]	GSE211414
Experimental models: Cell lines		
JM8A3 murine embryonic stem cells	EuMMCR	https://www.eummcr.info
Experimental models: Organisms/strains		
B6(Cg)-Tyrc-2J/J	JAX	Cat# JAX:000058, RRID:IMSR_JAX:000058
C57BL/6JRccHsD	Inotiv	https://www.inotiv.com/
Tg(Cd4-cre)1^{Cwi} (CD4-Cre)	JAX	Published in Lee et al.[43]
Cd4$^{tm1(cre/ERT2)Thbu}$ (CD4-CreERT2)	Thorsten Buch, UZH Zürich	Published in Śledzińska et al.[36]
Rag2^{tm1Fwa} (Rag2$^{-/-}$)	JAX	Published in Shinkai et al.[74]
Gt(ROSA)26Sor$^{tm1(CAG-Satb1,-EGFP)Bey}$ (R26-STOP-Satb1)	This Paper	ND
Satb1^{em1Bey} (Satb1$^{fl/fl}$)	This lab	Published in Sommer et al.[35]
Foxp3^{tm1Flv} (Foxp3-RFP)	JAX	Cat# JAX:008374, RRID:IMSR_JAX:008374
Oligonucleotides		
Oligonucleotide Sequences	This paper	Table S3
Recombinant DNA		
R26-STOP-Satb1	This paper	ND
STOP-eGFP-ROSA targeting vector	Thomas Wunderlich	Published in Sasaki et al.[75]

(*Continued on next page*)

Continued

REAGENT or RESOURCE	SOURCE	IDENTIFIER
Software and algorithms		
Agilent Seahorse Wave Software	Agilent	RRID:SCR_014526
Bioconductor Packages (critical packages are stated in methods and figure)	Bioconductor	https://www.bioconductor.org, RRID:SCR_012915
Bowtie2 v2.3.5	Langmead et al.[76]	http://bowtie-bio.sourceforge.net/bowtie2/index.shtml, RRID:SCR_016368
CASAVA v1.8.2	Illumina	http://support.illumina.com/sequencing/sequencing_software/casava.html, RRID:SCR_001802
CRAN packages (critical packages are stated in methods and figure)	CRAN	http://cran.r-project.org/, RRID:SCR_003005
DeepTools v3.3.0	Ramirez et al.[77]	https://deeptools.readthedocs.io/en/develop/, RRID:SCR_016366
FastQC	FastQC	http://www.bioinformatics.babraham.ac.uk/projects/fastqc/, RRID:SCR_014583
FlowJo	Becton Dickinson	https://www.flowjo.com/, RRID:SCR_008520
GraphPad Prism	GraphPad Software	https://www.graphpad.com/, RRID:SCR_002798
Image Lab software. Version5.2.1 built11	Bio-Rad	RRID:SCR_014210
LightCycler Software	Roche	RRID:SCR_012155
MACS2 v2.1.2	Zhang et al.[78]	https://github.com/macs3-project/MACS, RRID:SCR_013291
Picard v2.9.2	Picard	http://broadinstitute.github.io/picard/, RRID:SCR_006525
R 3.5.3	R Project	http://www.r-project.org/, RRID:SCR_001905
R Studio	R Studio	https://posit.co/, RRID:SCR_000432
SAMtools v1.9	Li et al.[79]	http://htslib.org/, RRID:SCR_002105
Star v2.7.1a.	Dobin et al.[80]	http://code.google.com/p/rna-star/, RRID:SCR_015899
trimmomatic v0.36	Bolger et al.[81]	http://www.usadellab.org/cms/index.php?page=trimmomatic, RRID:SCR_011848
BD Rhapsody Sequence Analysis Pipeline 2.2.1	Becton Dickinson	https://bd-rhapsody-bioinfo-docs.genomics.bd.com/top_introduction.html
Bcl2fastq2 V2.20	Illumina	https://support.illumina.com/sequencing/sequencing_software/bcl2fastq-conversion-software.html, RRID: SCR_015058
MACS3	Zhang et al.[78]	https://github.com/macs3-project/MACS, RRID: SCR_013291
R 4.3.0	R Project	http://www.r-project.org/, RRID:SCR_001905
Seurat V4.3.0.1	Butler et al.[82]	https://satijalab.org/seurat/get_started.html, RRID:SCR_016341
Signac V1.10.0	Stuart et al.[83]	https://satijalab.org/signac/index.html, RRID:SCR_021158
SeuratWrappers V0.3.1	SeuratWrappers	https://github.com/satijalab/seurat-wrappers, RRID:SCR_022555
presto V1.0.0	presto	https://rdrr.io/github/immunogenomics/presto/
clusterProfiler V.4.8.1	Yu et al.[84]	http://bioconductor.org/packages/release/bioc/html/clusterProfiler.html, RRID:SCR_016884

(*Continued on next page*)

Continued

REAGENT or RESOURCE	SOURCE	IDENTIFIER
rrvgo V1.12.2	Sayols[85]	https://www.bioconductor.org/packages/release/bioc/html/rrvgo.html
Cicero V1.3.9	Pliner et al.[86]	https://cole-trapnell-lab.github.io/cicero-release/
JASPAR2020 V0.99.10	Fornes et al.[87]	https://rdrr.io/github/da-bar/JASPAR2020/, RRID:SCR_003030
ggplot2 V3.4.2	ggplot2	https://cran.r-project.org/web/packages/ggplot2/index.html, RRID:SCR_014601
eulerr V7.0.2	eulerr	https://cran.r-project.org/web/packages/eulerr/index.html, RRID:SCR_022753
BSgenome.Mmusculus.UCSC.mm10 V1.4.3	UCSC mm10	https://bioconductor.org/packages/release/data/annotation/html/BSgenome.Mmusculus.UCSC.mm10.html
EnhancedVolcano v1.18.0	EnhancedVolcano	https://bioconductor.org/packages/release/bioc/html/EnhancedVolcano.html RRID:SCR_018931
scCustomize V1.1.1	scCustomize	https://rdrr.io/cran/scCustomize/, RRID:SCR_024675
gt V0.11.1	gt	https://rdrr.io/cran/gt/
AnnotationHub V3.8.0	AnnotationHub	https://rdrr.io/bioc/AnnotationHub/, RRID:SCR_024227
GenomicRanges V1.52.0	Lawrence et al.[88]	http://www.bioconductor.org/packages/2.13/bioc/html/GenomicRanges.html, RRID:SCR_000025
TFBSTools V1.38.0	Tan et al.[89]	https://bioconductor.org/packages/TFBSTools/, RRID:SCR_024260
ggseqlogo V0.2	ggseqlogo	https://rdrr.io/cran/ggseqlogo/
Custom code	This paper	https://doi.org/10.5281/zenodo.15201055
Other		
MOG38–49/I-Ab (GWYRSPFSRVVH) BV421	NIH	N/A

EXPERIMENTAL MODEL AND STUDY PARTICIPANT DETAILS

Mice

Mice (crossed more than 7-times to a C57BL/6JRcc background) were housed under specific pathogen-free conditions with chow and water provided *ad libitum*. Mice were used in accordance with the local legislation governing animal studies following The Principles of Laboratory Animal Care (NIH publication No. 85-23, revised in 1996). All animal experiments were approved by the Local Animal Care Commission of North Rhine-Westphalia (AZ 84-02.04.2013.A248 and AZ 84-02.04.2016.A370). Unless otherwise denoted, mice were used for experiments between nine weeks and four months of age and cohorts were age and sex matched.

C57BL/6JRcc, Satb1$^{fl/fl}$, CD4-Cre, CD4-CreERT2 and RAG2$^{-/-}$ mice were previously described.[35,36,43,74] Conditional R26-STOP-Satb1 mice were generated for this study (see Figure S5).

For experiments the following genotypes were used: R26-STOP-Satb1$^{wt/+}$ x CD4-Cre$^{wt/+}$ as KI mice or R26-STOP-Satb1$^{wt/+}$ x CD4-Cre$^{wt/wt}$ as WT control. Unless otherwise denoted Satb1$^{fl/fl}$ x CD4-CreERT2$^{wt/+}$ mice were used for conditional deletion of Satb1. Mice were either treated with tamoxifen (KO) or oil as control (WT). Experimental autoimmune encephalomyelitis (EAE) was induced in 14 weeks old female Satb1$^{fl/fl}$ x CD4-CreERT2$^{+/wt}$ or Satb1$^{fl/fl}$ x CD4-CreERT2$^{wt/wt}$ mice. Both cohorts were treated with tamoxifen. The influence of long-term deletion of Satb1 was studied in 44-60 weeks old Satb1$^{fl/fl}$ x CD4-Cre$^{wt/+}$ mice and Satb1$^{fl/fl}$ x CD4-Cre$^{wt/wt}$ as control. For the experimental colitis model male Rag2$^{-/-}$ mice were used.

Primary cells and cell lines

JM8A3 murine embryonic stem cells (EuMMCR) were cultured on mitomycin C-inactivated and G418 resistant mouse embryonic fibroblast feeder layers in DMEM supplemented with 15% heat-inactivated fetal calf serum, 1% non-essential amino acids, 1% Glutamax, 1 mM Sodium Pyruvate, 0,1 mM β-Mercaptoethanol, 100 U/ml Penicillin, 100 μg/ml Streptomycin and LIF under standard

murine ES cell culture conditions as described previously.[35] JM8A3 cells were tested for mycoplasma contamination before blastocyst injection. Primary murine splenocytes or $CD4^+$ T cells were cultured in IMDM (Gibco) supplemented with 10% FCS, 1% non-essential amino acids, 1% Glutamax, 5 mM HEPES, 0.5 mM sodium pyruvate, 55 μM β-mercaptoethanol, 100 U/ml Penicillin and 100 μg/ml Streptomycin. All cells were cultivated at 37°C, 5%CO2.

Microbe strains

For genetic engineering, two different E.coli strains were used: DH5α (DSMZ) and Stbl3 (Thermo Fisher Scientific). Bacteria were cultivated in LB-medium containing plasmid-specific antibiotics.

METHOD DETAILS

Generation of Satb1-overexpressing mice

To generate Satb1-overexpressing mice, the Satb1 coding region was amplified via PCR and integrated into an AscI-linearized STOP-eGFP-ROSA targeting vector[75] using standard gene cloning procedures. Correct insertion was verified by sequencing and subsequently the EcoRI-linearized targeting vector was electroplated into JM8A3 murine embryonic stem cells for homologous recombination. ES cell transfection, cultivation and G418 selection was performed as previously described.[35] Recombinant ES cells were screened by PCR (Primer sequences are listed in Table S3) and Southern blotting for correct integration. Southern Blot procedure was described previously in detail.[35] For validation of correct 5' integration, DNA was digested with EcoRI-HF (NEB), while for internal screening DNA was digested with KpnI-HF (NEB) when Southern Blot was performed. Probes were generated by enzymatic digestion and either radioactively or DIG-labeled. Positive ES clones were injected into B6(Cg)-Tyrc-^{2J}/J blastocysts (Jackson strain 000058) to generate chimeric mice. Chimeric mice were mated with C57BL/6JRcc mice and transgenic offsprings were backcrossed to C57BL/6JRcc background. Subsequently, R26-STOP-Satb1 mice were crossed to CD4-Cre mice to induce Satb1 overexpression in CD4 expressing cells.

Tamoxifen administration

Tamoxifen (Merck) was dissolved to a final concentration of 40 mg/ml in pre-heated olive oil (Merck, 55°C). To induce Cre-mediated recombination, 8 mg tamoxifen were administered to Satb1$^{fl/fl}$ x CD4-CreERT2$^{wt/+}$ animals by oral gavage on day 0 and on day three. Unless otherwise mentioned, seven days after initial tamoxifen administration, mice were either scarified for $CD4^+$ T cell isolation or EAE was induced. For suboptimal Satb1 deletion *in vivo*, 5 mg tamoxifen were administered to Satb1$^{fl/fl}$ x CD4-CreERT2$^{wt/+}$ animals by oral gavage only on day 0 thereby inducing gene deletion at a reduced efficiency.

For cell isolation, control mice received olive oil instead of tamoxifen. For EAE experiments, female Satb1$^{fl/fl}$ x CD4-CreERT2$^{wt/wt}$ animals were used as control and mice received tamoxifen similar to Satb1$^{fl/fl}$ x CD4-CreERT2$^{wt/+}$ animals, since tamoxifen administration itself influence EAE induction.[36,90]

To delete Satb1 *in vitro*, T cells from Satb1$^{fl/fl}$ x CD4-CreERT2$^{wt/+}$ animals were treated with 1 μM 4-OH tamoxifen (Merck), which was previously solved in EtOH. As wildtype control, cells were treated with EtOH at the same final concentration.

Induction and assessment of experimental colitis

Satb1$^{fl/fl}$ x CD4-CreERT2$^{wt/+}$ mice were treated with tamoxifen or oil as control as described above and splenic $CD4^+CD44^-CD62L^+CD25^-$ naive T cells were isolated. Colitis was induced by the adoptive transfer of $1x10^6$ naive $CD4^+$ T cells intraperitoneally (i.p.) into Rag2$^{-/-}$ animals. As control, Rag2$^{-/-}$ mice were only injected with PBS. Recipient mice were weight 3 times a week and monitored for signs of illness. When colitis symptoms manifested, approximately five weeks after naive $CD4^+$ T cell injection, mice were sacrificed by cervical dislocation and cells were analyzed by flow cytometry and colon was prepared for histological analysis.

Induction of experimental autoimmune encephalomyelitis (EAE)

EAE was induced by active immunization of mice with myelin oligodendrocyte glycoprotein (MOG) 35-55 peptide (MOG_{35-55}) and complete Freund's adjuvant as described previously.[91] In brief, 1 μg/μl MOG_{35-55} (Biotrend) was dissolved in PBS with 1% dimethyl sulfoxide and emulsified 1:1 with complete Freund's adjuvant (BD) supplemented with 10 mg/ml Mycobacterium tuberculosis H37RA (BD). Mice were anesthetized with 2.5-3.5% isoflurane and immunized with 50 μg of MOG_{35-55} by tail-base injection. Subsequently, mice received i.p. 200 ng pertussis toxin (Merck) diluted in PBS on day 0 and on day two.

Mice were monitored daily and clinical score was assessed using the following score: 0 = no clinical sign, 0.5 = reduced tail tonicity, 1 = loss of tail tonicity, 1.5 = loss of tail tonicity and unilateral hindlimb weakness, 2 = loss of tail tonicity and bilateral hindlimb paresis, 2.5 = loss of tail tonicity and unilateral hindlimb paralysis, 3 = loss of tail tonicity and bilateral hindlimb paralysis. Upon clinical score 0.5, soaked food was placed on the cage floor. If mice reached a clinical score above 3, showed great pain or lost more than 20% of their initial bodyweight, they were excluded from the experiment and euthanized for animal welfare reasons. At peak of disease, occurring on day 18, cells were isolated from different tissues as described below or spinal cord was prepared for histological analysis.

Isolation of immune cells

Cells were purified from spleen, cLN, mesLN, colon, small intestine and CNS. For lymphocyte isolation out of the spleen and lymph nodes, organs were manual homogenized into a single-cell suspension and passed through a 100 μm cell strainer. Splenocytes were cleared form erythrocytes by incubating cells in red blood cell lysis buffer (155 mM NH_4Cl, 10 mM $KHCO_3$, 0.1 mM EDTA, pH 7.2-7.4) for 2 min. Cells were washed in PBS and directly used for further experiments. For isolation of myeloid cells, spleens were cut into small pieces and digested in 3 ml RPMI supplemented with 0.5 mg/ml Collagenase Type IV (Merck) and 50 μg/ml DNAseI (Merck) for 45 min at 37°C with slow rotation. After digestion, remaining pieces were manual homogenized, cell suspension was filtered and red blood cell lysis was performed as described above. Isolation of mononuclear cells from the CNS was performed as described previously.[91] After perfusion of the animals with PBS, brain and spinal cord were removed, cut into small pieces and digested in 5 ml DMEM supplemented with 10% FCS and 200 μg/ml Collagenase Type IV (Merck) for 45 minutes at 37°C followed by digesting with 170 μg/ml DNaseI (Merck) for 45 minutes at 37°C under slow rotation. The homogenized tissue was passed through a 100 μm cell strainer and lymphocytes were isolated using density gradient centrifugation (20 min, 900 g, room temperature). Cells were collected from the 30%/70% interphase of the percoll gradient, washed in PBS and further used for FACS staining or stimulated to assess cytokine production. Isolation of intestinal lamina propria mononuclear cells was performed as described previously.[92] Colon and small intestine were collected, flushed with PBS and residual mesenteric fat and Peyer's patches were removed. The intestine was opened longitudinally and cut into pieces of approximately 1 cm length. The sample was incubated in HBSS supplemented with 5 mM DTT, 2% FCS, 100 U/ml Penicillin and 100 ug/ml Streptomycin for 20 min at 37°C with slow rotation for mucosal removal, followed by incubation in HBSS containing 5 mM EDTA, 2% FCS, 100 U/ml Penicillin and 100 μg/ml Streptomycin for three times 15 min at 37°C with slow rotation for epithelial cell removal. The tissue was washed in HBSS supplemented with 10 mM HEPES, 100 U/ml Penicillin and 100 μg/ml Streptomycin for 10 min at 37°C with slow rotation, cut into smaller pieces and digested in HBSS supplemented with 0.2 U/ml Liberase (Merck), 200 U/ml DNaseI, gradeII (Merck), 10 mM HEPES, 100 U/ml Penicillin and 100 ug/ml Streptomycin for 45 min at 37°C with slow rotation. Cell suspension was filtered through a 70 μm cell strainer and washed three times with HBSS containing 2% FCS. Cells were used immediately for FACS staining or stimulated to determine the cytokine profile.

Isolation of naive and effector/memory $CD4^+$ T cells

Splenocytes and lymph node cells were pooled and $CD4^+$ T cells were enriched by negative selection using the MagniSort Mouse CD4 T cell enrichment Kit (Thermo Fisher Scientific) according to the manuscript. Subsequently $CD4^+$ T cells were surface stained with anti-CD3, anti-CD4, anti-CD25, anti-CD62L and anti-CD44 and naive $CD3^+CD4^+CD25^-CD44^{low/-}CD62L^+$ T cells and effector/memory $CD3^+CD4^+CD25^-CD44^{high}CD62L^-$ T cells were sorted on a BD FACS Aria III to greater than 98% purity.

In vitro $CD4^+$ T cell differentiation

Differentiation of naive $CD4^+$ T cells was performed as previously described.[33] In brief, naive $CD4^+$ T cells were cultivated in 96- or 48-well plates coated with an anti-hamster IgG antibody (MP Biomedicals, 1:20), in presence of soluble anti-CD3ε (0.25 μg/ml, Biolegend, RRID:AB_312679) and anti-CD28 (1 μg/ml, Biolegend, RRID:AB_312877). For specific differentiation, the following cytokine and antibody mix were added: For T_H0 condition, anti-IL-4 (2 μg/ml, Biolegend, RRID:AB_315322) and anti-IFNγ (2 μg/ml, Biolegend, RRID:AB_315394) was added; For T_H1 cell differentiation, anti-IL-4 (2 μg/ml) and IL-12 (10 ng/ml, PeproTech) was added; For T_H2 cell differentiation, anti-IFNγ (2 μg/ml) and IL-4 (10 ng/ml, Immunotools) was added; For T_H17 cell differentiation, anti-IL-4 (2 μg/ml), anti-IFNγ (2 μg/ml), TGF-ß1 (0.3 ng/ml) and IL-6 (20 ng/ml, ImmunoTools) was added; For iT_{reg} cell differentiation, anti-IL-4 (2 μg/ml), anti-IFNγ (2 μg/ml), TGF-ß1 (2 ng/ml), IL-2 (100 U/ml, Chiron) and retinoic acid (2.5 nM, Merck) was added. When T_H0, T_H1 and T_H2 cells were cultured for longer than three days, cell were rested on day two in presence of IL-2 (100 U/ml). On day four, T_H0, T_H1 and T_H2 cells were restimulated in the corresponding conditions (s. above) for one day. Cells were cultivated for three or five days. For stimulation of mature T_H17 cells, T_H17 cells were rested after five days of cultivation for two days in complete IMDM without cytokine additives in presence of 1 μM 4-OH tamoxifen or EtOH as control and cells were restimulated at day seven under T_H17 conditions (s. above) for two days.

For T_H17 culture in presence of anti-IL-2 (10 μg/ml, Biolegend, RRID:AB_315294) and anti-CD25 (10 μg/ml, Biolegend, RRID:AB_312863), naive $CD4^+$ T cells were activated by plate bound anti-CD3ε (5 μg/ml), anti-CD28 (1 μg/ml) and cultured in presence of anti-IL-4 (10 μg/ml), anti-IFNγ (10 μg/ml), TGF-ß (5 ng/ml) and IL-6 (20 ng/ml) according to previous description.[93] For T_H17 cultures in the presence of human IL-2 (10, 100 IU/ml) and anti-mouse IL-2 (10 μg/ml, Biolegend, RRID:AB_312863), naive $CD4^+$ T cells were differentiated in 96-well plates coated with anti-hamster IgG antibody in presence of soluble anti-CD3ε and anti-CD28, anti-IL-4, anti-IFNγ, TGF-ß1 and IL-6. For iT_{reg} cell differentiation in the presence of anti-mouse IL-2 (10 μg/ml, Biolegend) and anti-CD25 (10 μg/ml, Biolegend), naive $CD4^+$ T cells were activated by plate bound anti-CD3ε (5 μg/ml), anti-CD28 (1 μg/ml) and cultured in the presence of anti-IL-4 (2 μg/ml), anti-IFNγ (2 μg/ml), TGF-ß1 (2 ng/ml) and retinoic acid (2.5 nM, Merck) and decreasing concentrations of IL-2 (100 IU [normal culture condition], 20 IU [low IL-2], no IL-2).

Proliferation assays

$CD4^+$ T cells were labeled with 5 μM cell proliferation dye eFluor670 (Thermo Fisher Scientific) for 10 min at 37°C according to the manufacturer's protocol. Cells were stimulated for 3 days with mouse T-Activator CD3/CD28 Dynabeads (Thermo Fisher Scientific) in a 3:1 cell/bead ratio and subsequently dilution of eFluor670 was measured by flow cytometry.

Labeling of CD4$^+$ T cells with PKH26 or eFluor670 for co-culture experiments

Naive CD4$^+$ T cells were sorted from the spleen and cLN of WT and KO mice as previously described. WT cells were labeled with PKH26 at a final concentration of $2x10^{-6}$ M of PKH26 at a density of $1x10^7$ cells/ml for 5 minutes at room temperature according to the manufacturer's recommendations (Sigma-Aldrich). KO cells were labeled with 5 μM cell proliferation dye eFluor670 (Thermo Fisher Scientific) as described before. Cells were either cultured alone or mixed at a 1:1 ratio and cocultured for 3 days under T_H17 cell differentiation conditions.

In vivo BrdU labeling of T cells and anti-BrdU staining to assess cell proliferation

Mice were injected intraperitoneally (i.p.) with BrdU solution (1mg/mouse) 72 hours prior to analysis. Splenocytes were isolated and stained with anti-BrdU antibodies according to the manufacturer's protocol (Biolegend). In short, cell surface proteins were stained and cells fixed on ice for 20 minutes by adding 100 μl Buffer A. Afterwards the cells were permeabilized by incubation of the cells in Buffer C for 10 minutes at room temperature. Then, the cells were fixed again for 5 minutes and treated with DNAse for 1 hour at 37°C. The cells were stained with anti-BrdU antibody for 20 minutes at room temperature in the dark prior to analysis by flow cytometry.

Analysis of metabolic parameters

Real-time metabolic parameters were measured using a Seahorse XFe96 Analyzer (Agilent). Analysis of the metabolic state of CD4$^+$ T cells upon TCR stimulation was performed as previously described,[94] CD4$^+$ T cells were purified by negative selection using the MagniSort Mouse CD4 T cell enrichment Kit (Thermo Fisher Scientific) and seeded on poly-L-lysine-coated (100 μg/ml, Merck) Seahorse cell culture microplates (Agilent) with a concentration of 300,000 cells/well. Cells were then incubated for one hour in Seahorse assay medium (Seahorse XF RPMI Medium supplemented with 2 mM L-glutamine, 1 mM sodium pyruvate, 10 mM glucose, adjusted to pH 7.4 prior to the assay) at 37°C without controlled CO_2 concentration. Baseline measurement was performed for four cycles and subsequently cells were stimulated with soluble anti-CD3ε/anti-CD28 antibody (Biolegend, RRID:AB_312679, RRID:AB_312877) at a final concentration of 3 and 1 μg/ml respectively. The extracellular acidification rate (ECAR) was measured for 19 cycles. Each measurement cycle was defined as three minutes mixing time and five minutes measurement time.

For the analysis of the metabolic state of T_H17 cells, cells cultured for three days under T_H17 cell skewing conditions were collected and 100,000 cells/well were seeded on a poly-L-lysine-coated Seahorse cell culture plates. Cells were either incubated for one hour in Seahorse assay medium (s. above) or glucose-free Seahorse assay medium at 37°C without controlled CO_2 concentration.

Three baseline measurements of the ECAR and the oxygen consumption rate (OCR) were performed prior to metabolic challenges. Each measurement cycle was defined as three minutes mixing time and three minutes measurement time. For challenges of mitochondria, cells were stimulated with (1) 1 μM oligomycin (Merck), (2) 4 μM FCCP (Merck) and (3) 0.5 μM rotenone (Merck) and 0.5 μM antimycin A (Merck). To analyze the response to glucose stimulation, cells were stimulated with (1) 10 mM glucose, (2) 1 μM oligomycin (Merck) and (3) 100 mM 2DG (Merck). During each stimulation period, three measurement cycles were performed. Normalization of the plate was performed by reading the absorbance at 590 nm of PFA-fixed, crystal violet stained cells after the assay performance.

Antibodies, staining and flow cytometry analysis

Fluorescent-labeled antibodies were purchased from BD Bioscience, Biolegend or Thermo Fisher Scientific. $MOG_{38–49}$/I-A^b tetramer (GWYRSPFSRWH) was obtained from the NIH Tetramer core facility. Surface staining was performed at 4°C for 20 min. To exclude dead cells, cells were stained with the LIVE/DEAD Fixable Dead Cell Stain Kit (Thermo Fisher Scientific) according the manufacturer's protocol. For intracellular cytokine staining, cells were first stained for surface marker expression as described above and subsequently stimulated with PMA/Ionomcyin (1:500, eBioscience Cell stimulation cocktail, Thermo Fisher Scientific) for four hours at 37°C in presence of Brefeldin A (1:1000, Thermo Fisher Scientific) and Monensin (1:1000, Thermo Fisher Scientific). Afterwards dead cells were stained as described above, cells were fixed with 4% paraformaldehyde for 10 min on ice, permeabilized using the ebioscience Permeabilization Buffer (Thermo Fisher Scientific) and intracellular stained for cytokines for 30 min at room temperature in Permeabilization Buffer. Transcription factors were stained using the Foxp3 / Transcription Factor Staining Buffer Set (Thermo Fisher Scientific) according to the manufacturer's protocol. For tetramer staining, cells were incubated with 20 μg/ml $MOG_{38–49}$/I-A^b tetramer for three hours at 37°C in RPMI (containing 10% FCS). Subsequently, cells were washed and stained for surface marker expression and dead cells as described above. To stain phosphorylated Stat proteins, cell were fixed with 3% methanol free formaldehyde (Thermo Fisher Scientific) for 10 min at 37°C, permeabilized in ice cold 90% methanol overnight at -20°C and subsequently stained for phosphorylated Stat proteins and surface marker expression in FACS buffer (0.5% BSA in PBS) for one hour at room temperature. Only antibodies which were resistant to the fixation and permeabilization treatment were used. All stainings were performed in presence of FcR-blocking reagents (anti-CD16/CD32, Biolegend, RRID:AB_312801). Flow cytometric acquisition was performed on a LSR II (BD), Symphony A5 flow cytometer (BD) or FACSAria III (BD) and data were analyzed using FlowJo software package (BD).

Immunoblot analysis for Satb1

Cells were lysed in RIPA buffer (10 mM Tris-HCl (pH 8), 1 mM EDTA (pH 8), 140 mM NaCl, 1% Triton X-100, 0.1% SDS, 0.1% Na-DOX in H_20) supplemented with cOmplet Protease Inhibitor Cocktail (Roche, Complete Mini) for 30 min on ice followed by three times sonication for 10 seconds at 20 V. Protein concentration was determined using the Pierce bicinchoninic acid assay (BCA) Protein Assay

Kit (Thermo Fisher Scientific) according to the manufacturer's protocol and absorbance was measured with the Infinite M200 multimode microplate reader or FLUOstar Omega. Per sample, 20 μg proteins were denatured at 70°C for 10 min in the presence of NuPAGE sample reducing agent (Thermo Fisher Scientific) and NuPAGE LDS sample buffer (Thermo Fisher Scientific) according to the manufacturer's instructions. Cell lysate was subjected to immunoblot analysis as previously described.[95] The following antibodies were used: anti-Satb1 (1:5000, Abcam) and anti-ß-actin (1:5000, Merck Millipore).

Histology

For histology analysis of the colon, the tissue was washed, fixed in 4% paraformaldehyde and embedded in paraffin using routine procedures. Sections were stained with hematoxylin und eosin and scored for disease progression as described previously.[96] Briefly, scores were assigned from 0 - 3 in 5 different categories: (1) number of follicle aggregates, (2) oedema, (3) erosion and ulceration, (4) crypt loss and (5) infiltration of mono- and polymorphonuclear cells. Furthermore, the (6) percentage of the involved area was assigned a score from 0-4. All scoring was performed by researchers blinded to the experimental conditions. For histological analysis of immune cell infiltration of the CNS, mice were perfused with PBS and 4% paraformaldehyde. The spinal cord was excised and further fixed in 4% paraformaldehyde and embedded in paraffin using routine procedures. Sections were prepared and stained with hematoxylin und eosin, anti-MAC3 (BD Biosciences) and anti-CD3 (Bio-Rad Laboratories) as described previously.[97] For histological analysis of myelin, spinal cords were dissected and fixed in 4% paraformaldehyde. Subsequently, samples were incubated in 30% sucrose and embedded in cryoembedding matrix. Sections (12 μm) were prepared using the CryoStar NX70 (Thermo Fisher Scientific), dehydrated in 95% ethanol and myelin was visualized using luxol fast blue staining (0.95% (w/V) Solvent blue 38 (Merck), 90% Ethanol, 0.47% Acetic acid in H_2O) overnight at 60°C. Samples were incubated in 0.05% lithiumcarbonat solution, 70% ethanol and H_2O multiple times until good contrast was archived. Subsequently, nuclear fast red (Merck) staining was performed for 2 min. Samples were washed in H_2O, dehydrated in 95% ethanol and 100% ethanol, cleared in Xylene. Histological analysis was conducted using a BZ-9000 (Keyence) microscope.

Quantitative RT-PCR

Total RNA was isolated from cells lysed in QIAzol reagent (Qiagen) by standard phenol/ chloroform extraction or using the Direct-zol-96 RNA kit (Zymo Research) according to the manufacture's protocol. cDNA was generated with the Transcriptor First Strand cDNA synthesis kit (Roche Diagnostics) and qRT-PCR was performed using the LightCycler 480 Probe Master (Roche) and the Universal Probe Library set (Roche) according to manufacturer specifications. qRT-PCR were run on a LightCycler 480 II (Roche) and analyzed using the LightCycler 480 Software, v1.5. Samples were normalized to the expression of β-actin. All PCR primer sequences and probes are listed in Table S3.

Transcriptome analysis of naive CD4$^+$ T cells

Total RNA was isolated from splenic naive CD4$^+$ T cells lysed in QIAzol Lysis Reagent (Qiagen) using the miRNeasy Micro Kit (Qiagen) according to the manufacturer's protocol. RNA quality and concentration was measured on the Agilent Tapestation 2200 (Agilent) using RNA screen tapes (Agilent) and further processed for barcoding, multiplexing and cDNA library construction using the TruSeq RNA Sample Preparation Kit v2 (Illumina). For indexing, barcoding indexes of Set A were used. cDNA library was measured in quality and quantity on Agilent Tapestation 2200 (Agilent) using High sensitivity Screen Tape (Agilent) and sequencing (single read, 75 bp) was performed on an Illumina HiSeq 1500 platform using the TruSeq SBS Kit v3 (Illumina) and TruSeq SR Cluster Kit v2 (Illumina) according to the manufacturer's instruction. Base calling and de-multiplexing were performed using CASAVA v1.8.2 and fastQC was used for quality control. Subsequently, the reads were aligned to the mm10-based mouse Gencode reference transcriptome vM16 and quantified on gene level using STAR v2.7.1a.[80] Gene expression quantifications were imported to R 3.5.3 (2019-03-11) and DESeq2 v1.22.2 was used for downstream analyses.[98] Lowly expressed genes (rowSums > 10) were filtered and variance stabilizing transformation was performed. Subsequently, principal component analysis was conducted on all present genes using the prcomp function (R/stats 3.5.3). Differential expression analysis was performed comparing WT and KO samples without pre-defined fold change threshold and using independent hypothesis weighting (IHW, v1.10.1)[99] as the multiple testing procedure. Genes with an adjusted p-value < 0.05 and a fold change >1.5 were determined as significantly differentially expressed. Functional enrichment analysis using the MSigDB data base[100] was performed on the DE gene sets using the R package ClusterProfiler v3.10.1.[84] The raw sequence data has been deposited to GEO with accession number GSE250577.

Analysis of Satb1 dependence on RORγt and Stat3

To assess dependency of Satb1 expression on Stat3 and RORγt expression and binding to the genomic Satb1 locus, we assessed publicly available RNA-seq, expression array and ChIP-seq datasets (GEO GSE40918, GSE23681. GSE21670, GSE40918, GSE229377, GSE38704, GSE70108, GSE190538, GSE211414).

Single-cell RNA-seq of CD4$^+$ T cells in EAE

CD4$^+$ T cells were sorted from the brain and spinal cord of WT and KO mice. Prior to sorting, each sample was labelled with a unique hashtag oligo (HTO)-conjugated anti-CD45 antibody (BD Mouse Immune Single-Cell Multiplexing Kit, #633793). CD4$^+$ T cells from

WT and KO mice were each loaded on a separate BD Rhapsody cartridge (BD Bioscience, #400000847) using a BD Rhapsody Express Single-Cell Analysis System. Cell and bead loading, cell lysis, bead recovery, reverse transcription, and exonuclease treatment were performed according to the manufacturer's instructions (BD Biosciences). As for library prep, targeted enrichment of 400 genes was performed using a selected panel of primers, which was followed by index PCR to ligate sequencing adapters. Quantification of the cDNA libraries was carried out using a Qubit Fluorometer with the Qubit dsDNA HS Kit (ThermoFisher), whereas the size distribution of the libraries was assessed using the Agilent High-Sensitivity D5000 assay on a TapeStation 4200 system (Agilent Technologies). Paired-end sequencing (2x75 cycles) was performed on a NextSeq 500 System (Illumina) using NextSeq 500/550 High Output Kit v2.5.

Raw bcl files were demultiplexed using the Bcl2fastq2 V2.20 from Illumina. Sequencing adapters were trimmed and sequencing reads with a PHRED score >20 were filtered using Cutadapt 1.16. Subsequently, STAR[80] was used to align reads against GENCODE vM16 mouse reference genome. Drop-seq tools 2.0.0 were used to generate a UMI-corrected gene expression count matrix. HTO sequences were added to the reference genome to allow for their retrieval during alignment. Downstream analysis was performed in R (version 4.0.3). The dataset was filtered using the barcodeRanks() function to exclude cells with unique molecular identifier (UMI) counts below the inflection point, representing the transition in UMI counts between cell-containing wells and empty wells. Downstream analysis was performed using the Seurat R package (version 3.9.9.9032).[101] The dataset was further filtered to exclude cells expressing a detected number of genes >50 and <150, and a detected total count of >100 and <2500. No filtering was performed based on mitochondrial genes since they were not included in the targeted gene panel. After such filtration, 10,002 cells were used for subsequent analysis.

$CD4^+$ T cells sorted from WT and KO mice were loaded on two separate cartridges. The aforementioned quality-control steps were performed on the joint dataset comprising both genotypes. To mitigate technical artifacts arising from the parallel experimental processing, we applied the Harmony package[102] for batch correction coupled with SCTransform for normalization. First, the dataset was split by genotype, and SCTransform was applied on each genotype independently. Then, integration features were computed using the SelectIntegrationFeatures function from Seurat. This was followed by merging the SCTransform-normalized objects, setting variable features to the integration features, and performing principal component (PC) analysis using the RunPCA function from Seurat. Harmony was then applied using RunHarmony, setting the "reduction" argument to "pca".

For clustering, FindNeighbors was used while setting the "reduction" argument to "harmony" and selecting 23 PCs, and FindClusters was used a resolution of 0.36. FindSubCluster was used to refine the clustering of T_H17 cells. To find differentially expressed genes across clusters, FindAllMarkers was used while setting min.pct to 0.2 and logfc.threshold to 0.25, and using the default Wilcoxon Rank Sum test. To define differentially expressed genes across genotypes for a given cluster, a new column was created in the metadata comprising the information on the cluster identity and genotype, and FindMarkers was used while setting ident.1 and ident.2 to the same cluster originating from WT vs. KO, and setting min.pct and logfc.threshold to 0.1 and 0.5, respectively. Of note, *Satb1* and *Cd4* were left out of the feature list used for differential expression analysis, since WT cells consistently had an elevated expression of *Cd4* due to the loss of one copy of *Cd4* in the CD4-CreERT2-expressing KO cells. Conversely, *Satb1* expression was consistently higher in KO cells since the primer used for its amplification targets the gene's UTR, meaning a higher detection rate among KO cells (i.e. Cre-driven *Satb1* recombined allele has two "correct-frame" UTRs). Heatmaps were generated using the pheatmap package. To generate gene-expression scatterplots, To generate gene-expression scatterplots, we first applied Seurat's AverageExpression function [followed by log1p transformation of the averaged values] on each cluster per genotype. In addition, we used FindMarkers to find differentially expressed genes across genotypes for each cluster as described above. Labelled genes in the scatterplots passed the thresholds of i) log2FC greater than 0.5 across genotypes, and ii) an average expression value of >1 in WT or KO. The raw sequence data has been deposited to GEO with accession number GSE250578.

Assay for Transposase accessible chromatin (ATAC)-Sequencing of naive $CD4^+$ T cells

ATAC-seq was performed according to already described protocols.[103,104] In brief, 60,000 naive $CD4^+$ T cells were lysed in 50 μl cold lysis buffer (10 mM Tris-HCl, pH 7.4, 10 mM NaCl, 3 mM $MgCl_2$, 0.1% IGEPAL CA-630) and immediately centrifuged at 500 g for 10 min. Transposase reaction was performed with in-house Tn5 Transposase in tagmentation buffer (10 mM TAPS-NaOH (pH 8.5), 5 mM MgCl2, 10% DMF) for 30 minutes at 37°C and purified using the MinElute PCR Purification Kit (Qiagen) according the manufacturer's protocol. Transposed DNA fragments were amplified using the NEBNext High-Fidelity PCR Master Mix (NEB) and customized Nextera PCR primers 1 and 2 (Primer sequences are listed in Table S3). The PCR products were purified using the MinElute PCR Purification Kit. Quality check and measurement of PCR concentration was performed on the Agilent Tapestation 2200 using High sensitivity D1000 Screen Tape (Agilent). Libraries were sequenced (single read, 75 bp) on an Illumina HiSeq1500 using the TruSeq Rapid SBS Kit (Illumina) and TruSeq Rapid Cluster Kit (Illumina) according to the manufacturer's instruction. After quality inspection of primary data using FastQC v 0.11.8 (https://www.bioinformatics.babraham.ac.uk/projects/fastqc/), adapter and low-quality sequences were trimmed using trimmomatic v0.36[81] and reads were aligned to reference mouse genome mm10 using Bowtie2 v2.3.5.[76] Picard v2.9.2 (http://broadinstitute.github.io/picard/) was used to identify duplicated reads and removal of Tn5 offset was performed using the alignmentSieve functionality of the deepTools suite v3.3.0.[77] Bam files were sorted and indexed using SAMtools v1.9.[79] After subsampling the reads for each sample to $5x10^6$ reads using Sambamba v0.7.0, normalized bigwig files were produced using deeptools v3.3.0 for genomic visualization of the read coverage. Subsequently, peaks were called with MACS2

v2.1.2.[78] After peak calling, bed files listing narrow peaks were imported to R 3.5.3 (2019-03-11) and consensus peak regions across all samples were generated with the 'reduce' function of the Bioconductor GenomicRanges package v1.34.0 and reads were counted per sample using the 'summarizeOverlaps' function of the Bioconductor GenomicAlignments package v1.18.1.[88] Genomic regions on the ENCODE blacklist for mm10 were excluded from the analysis. ChIPseeker v1.18.0 was used to annotate genomic regions[105] using the TxDb.Mmusculus.UCSC.mm10.knownGene data base v3.4.4. Peak regions were filtered for a minimum sum of 10 counts across all samples and a minimum MACS2 detection rate of at least 2 samples per group. After normalization using the Bioconductor DESeq2 package v1.22.2,[98] variance stabilizing transformation was performed and principle component analysis on all detected peaks was conducted using the prcomp function (R/stats 3.5.3). Subsequently, differentially accessible regions were determined using the DESeq2[98] and independent hypothesis weighting using the R package IHW v1.10.1.[99] Regions with an adjusted p-value < 0.1 and a fold change >1.5 were determined as significantly differentially accessible. Functional enrichment analyses were performed on the differentially accessible region sets using the gene ontology[106,107] and MSigDB[100] data bases with the R package ClusterProfiler v3.10.1.[84] ATAC-seq data can be accessed under GSE250576.

Single-cell ATAC-seq and whole transcriptome analysis of naive CD4$^+$ T cells and *in vitro* differentiated T_H1 and T_H17 cells

Nuclei from T_H1, T_H17, and naive T cells were isolated and labeled with the nuclear Sample Tag reagent (Ms nucleoporin p62 Sample Tag 5-9, #460293-460296). After tagmentation, 40,000 labeled single nuclei from WT and KO cells were loaded onto a BD Rhapsody 8-Lane Cartridge (BD Biosciences #666262) using the BD Rhapsody Express Single-Cell Analysis System. Single-cell capture, ligation, reverse transcription, and Exonuclease I treatment were performed in accordance with the manufacturer's recommendations (BD Biosciences). Whole transcriptome, ATAC and sample tag libraries were obtained according to the manufacturer's protocol (BD Biosciences). Quantification of the cDNA libraries size distribution of the libraries were carried out using a Qubit Fluorometer with the Qubit dsDNA HS Kit (ThermoFisher), and Agilent High-Sensitivity D5000 assay on a TapeStation 4200 system (Agilent Technologies), respectively. Paired-end sequencing was performed on a NovaSeq 6000 system using different parameters for mRNA/sample tag libraries and ATAC libraries. For mRNA and sample tag libraries, the following sequencing parameters were used: R1: 76 cycles, R2: 151 cycles, utilizing S4 Reagent Kits v1.5 (300 cycles). ATAC libraries were sequenced with these settings: R1: 50 cycles, R2: 50 cycles, Index 1: 8 cycles and Index 2: 60 cycles, employing NovaSeq 6000 S2 v1.5 (200 cycles) chemistry.

After demultiplexing of bcl files using Bcl2fastq2 V2.20 (Illumina) to generate fastq files, including both reads and indices specifically for ATAC libraries, the BD Rhapsody Sequence Analysis Pipeline 2.2.1 was used to align reads against the gencode mouse reference genome (M23) and generate molecular counts per bioproduct per identified nucleus and metrics related to the different steps [https://bd-rhapsody-bioinfo-docs.genomics.bd.com/top_introduction.html]. Downstream analysis was performed using the R packages Seurat (V4.3.0.1) and Signac (V1.10.0).[82,83,108] First, nuclei that could not be associated with a single HTO barcode were removed from the dataset. During quality control of the whole transcriptome data, nuclei that did not exceed 400 associated features or showed more than 10,000 features were excluded from downstream analysis. Additionally, only nuclei from naive CD4$^+$ T cells with less than 25% mitochondrial reads or from T_H1/T_H17 cells with less than 40% mitochondrial reads were retained. For chromatin accessibility data, peak calling with MACS3 was performed on nuclei passing the RNA quality control.[78] Then, only nuclei with more than 1,000, but less than 100,000 associated fragments, more than 20% of reads in peaks, a nucleosome signal of less than 4, a transcription start site (TSS) enrichment score of more than 3 and less than 5% of fragments in ENCODE blacklisted genomic regions were retained. After QC, a total of 48,110 nuclei were subjected to downstream analysis. The transcriptomic data was log-normalized, scaled and centered, followed by dimensionality reduction (PCA) on the top 5,000 variable genes as identified by the vst method. The 25 first principal components (PCs) were then used for uniform manifold approximation and projection (UMAP). The ATAC data was normalized by computing the term-frequency inverse-document-frequency (TF-IDF), followed by determining top features and running dimensionality reduction through singular value decomposition (SVD). Since a strong correlation between the first LSI (latent sematic indexing) component and the sequencing depth was observed, only components 2 to 20 were used for UMAP. Both modalities (RNA and ATAC) were integrated by constructing a weighted nearest neighbor (WNN) graph and UMAP based on the first 20 RNA PCs and LSI components 2-20.

T cell subtype- and genotype-specific transcript and region markers were calculated using the Wilcoxon rank sum test (min.pct = 0.1) of the presto-based implementation of the 'FindMarkers' function (SeuratWrappers V0.3.1, presto V1.0.0). For downstream analysis, only markers with a log2 fold change bigger than 0.25 or smaller than -0.25 as well as a bonferroni-adjusted p value of less than 0.05 (RNA) or 10e-5 (ATAC) were considered. Identified differentially accessible regions were assigned to a putative target gene based on proximity using the 'ClosestFeature' function. Enrichment analysis of the MSigDB mouse hallmark gene sets[100] and gene sets from the Gene Ontology (GO) biological process (BP) database[106,109] on differentially expressed genes and genes associated with differentially accessible regions was performed with the clusterProfiler package (V4.8.1).[84,110] Redundancy in the list of enriched GO Terms was identified with the package rrvgo (V1.12.2).[85] The top two terms of the four most abundant term groupings were chosen for visualization. Co-accessible networks based on ATAC data were calculated using Cicero (V1.3.9),[86] and motifs from the JASPAR2020 vertebrate collection (V0.99.10)[87] enriched in differentially accessible regions were defined using the 'FindMotifs' function.

QUANTIFICATION AND STATISTICAL ANALYSIS

All statistical analyses, except for the analyses of sequencing data, were performed with GraphPad Prism software v5-8 (GraphPad Software). When analyzing statistical differences between two groups, two-tailed unpaired Student's t-tests were performed. Statistical differences between three or more groups treated under similar conditions were analyzed by one-way ANOVA with Dunnett's or Tukey's multiple comparison tests. Two-way ANOVA were performed when comparing multiple groups in the context of different conditions. Sidak's or Tukey's multiple comparison tests were performed dependent of the experimental conditions. If the same cells or mice were measured at different time points, repeated measure analysis was performed. P values of less than 0.05 were considered to be significant (ns indicates not significant $p > 0.05$, $p < 0.05$ = *; $p < 0.01$ = **; $p < 0.001$ = ***). Descriptive statistics, the performed statistical tests as well as the number of samples are stated in the figure legends. Sequencing data were analyzed in R studio.